Chezoía

34rd Annual

American Helicopter Society

International Student Design Competition

Final Proposal UMD Undergraduate Student Team

UNIVERSITY OF MARYLAND

Alfred Gessow Rotorcraft Center

Department of Aerospace Engineering

University of Maryland

College Park, MD 20740 U.S.A

Andrew Desrochers

Undergraduate Student (Team Leader)

desrochersandrew@gmail.com

Andrew Dallas

Undergraduate Student

adallas1@umd.edu

Jeremy Foust

Undergraduate Student

jfoust13@terpmail.umd.edu

Scott Jordan

Undergraduate Student

scottajord@gmail.com

Students received credit for ENAE 482: Aeronautical Systems Design for their contributions.

Dr. James Baeder

Faculty Advisor

baeder@umd.edu

Dr. Vengalatore Nagaraj

Faculty Advisor

vnagaraj@umd.edu

Alfred Gessow Rotorcraft Center

Department of Aerospace Engineering

University of Maryland

College Park, MD 20740 U.S.A

To the American Helicopter Society:

The members of the University of Maryland Undergraduate Student Design Team hereby grant AHS full permission to distribute the enclosed Executive Summary and Final Proposal for the 33rd Annual Design Competition as they see fit.

Thank you,

The UMD Undergraduate Design Team

ACKNOWLEDGEMENTS

The *Chezoía* design team wishes to acknowledge the following people for their invaluable discussion, guidance, and support throughout the course of this project.

University of Maryland Faculty

Dr. James Baeder

Dr. Vengalattore T. Nagaraj

Dr. Inderjit Chopra

Dr. Derek Paley

Industry Professionals

Dr. Ashish Bagai - DARPA

Brent T. Mills – US Army Research Laboratory

Special thanks to:

Dr. Camli Badrya

Dr. Bharath Govindarajan

Dr. Vikram Hrishikeshavan

Dr. Joseph H. Schmaus

Tyler Sinotte

Will Staruk

Br. Marius Strom

Lauren Trollinger

Elizabeth Ward

Contents

List of Figures

List of Tables

Nomenclature

Symbol	Units	Description
A	ft^2	Rotor area
AoA	degrees	Angle of Attack
AR		Aspect ratio
C_L		Lift coefficient
C_P		Pressure coefficient
C_T		Thrust coefficient
D	lbs	Drag
D_e	lbs	Equivalent rotor drag
DL	lb/ft^2	Disk loading
FM		Figure of merit
GTOW	lbs	Gross takeoff weight
K		induced power factor
L	lbs	Lift
L_{AE}	lbs	Sound exposure level
MTOW	lbs	Maximum takeoff weight
μ		Advance ratio
ρ	$slugs/ft^3$	Air density
PL	lb/hp	Power loading
r	ft	Rotor radius
RFI		Request for Information
RFP		Request for Proposal
RPM	rot/min	Rotations per minute
σ		Solidity
SFC	lb/hp-hr	Specific fuel capacity
T	lb	Thrust
V_{BE}		Velocity for best endurance
V_{BR}		Velocity for best range
V_{max}		Maximum velocity

1 Introduction

The 2016 AHS Student Design Competition Request for Proposal (RFP) calls for an unoccupied aerial vehicle capable of carrying a non-productive payload of no less than 176.4 lb (80 kg) and hovering in a controlled manner for a cumulative duration of 24 hours spent between three hover stations. A summary of the key compliances with the RFP is found below in Table 1.1.

Table 1.1: RFP Compliance Summary.

RFP Requirement	Design Solution	Section
Vehicle shall be capable of hovering for 24 hours without landing	Low disk-loading multirotor design allows for 25 hours of hover	5.3-4
Payload capacity of 176.4 pounds (80 kg)	Central fuselage accommodates payload weight or an equivalent human pilot	7.3
Aircraft is unoccupied	Advanced avionics package allows for fully autonomous mission	10.3
Aircraft must hover inside 3 separate Hover Stations, no less than 0.54 nautical miles (1 km) apart	Aircraft flies at a top speed of 37 knots (19 m/s), with autonomous obstacle avoidance during flight	8.2
Hover within 65.6 feet (20 m) radius sphere	Control scheme and canted rotors attenuates gusts and returns to stable hover position within 2 feet (0.6 m)	11.3

The helicopter's ability to hover provides unique capabilities not provided by fixed wing aircraft. Unfortunately, helicopters in hover tend to require significantly more power than comparable fixed wing aircraft in forward flight. The 2016 AHS 24 Hour Hover Challenge encourages innovation in regards to hover efficiency. Three key design areas that can improve hover efficiency are empty weight fraction, efficient power generation, and rotor aerodynamics. Empty weight fraction can be improved through the use of lightweight structures allowing the helicopter to function more efficiently. Power generation efficiency can be improved through the use of fuels with high specific energy and engines with low specific fuel consumption or the use of renewable energy solutions. Designing rotors with low disk loading reduces the power required.

However, low disk loading introduces challenges of its own, especially in the areas of controllability and durability. The rotor sizes typically required for low disk loadings lead to slower response times to control inputs, thus reducing the capabilities for precision hover. Additionally, these large rotors are more subject to failures when compared to smaller rotors. A successful mission of 24 hours requires both durability and the availability of redundancies in the case of system failures over such a long time span.

Through the application of innovative design concepts and proven technology based on recent advances in lightweight structures, engine design, and hover efficient airfoils, the University of Maryland Design Team presents *Chezoía*, a distributed propulsion design that offers extreme hover efficiency for unprecedented hover duration. The name *Chezoía* is derived from the Greek

words chelóna and makrozoía, meaning turtle and longevity respectively. This portmanteau was created to highlight the aircraft's main mission, as well as reflect pride in the University of Maryland's mascot, the diamondback terrapin.

Chezoía has been designed with 18 rotors, in order to take advantage of the efficiency benefits of their low disk loading, while at the same time maintaining control response times and durability with smaller rotors. This involves the use of diesel electric hybrid propulsion as well as fixed pitch, variable RPM rotors arranged in a compact dual hexagon layout for ease of control. Additionally, to minimize structural weight, the microtruss structure from the *Gamera* human powered helicopter serves as the main trusses for the hexagonal design. For the facilitation of a fully autonomous mission, *Chezoía* has also been equipped with advanced vision and distance sensors, for dynamic adjustment during flight.

Table 1.2: Weight and design highlights.

Design Highlights	
GTOW	1003.4 lbs (455.1 kg)
Empty Weight	607.0 lbs (275.3 kg)
Payload Weight	176.4 lbs (80.0 kg)
Fuel Weight	220.0 lbs (99.8 kg)
Number of Rotors	18
Blades per Rotor	2
Rotor Diameter	11.0 ft (3.35 m)

The design philosophy used during development concentrated on the key parameters of hovering efficiency, durability, controllability, and versatility while using currently available technologies to drive innovative solutions.

2 Mission Requirements

The mission provided by the RFP is to hover for a cumulative duration of 24 hours inside three separate Hover Stations following takeoff without landing, assuming sea level standard conditions as shown in Figure 2.1.

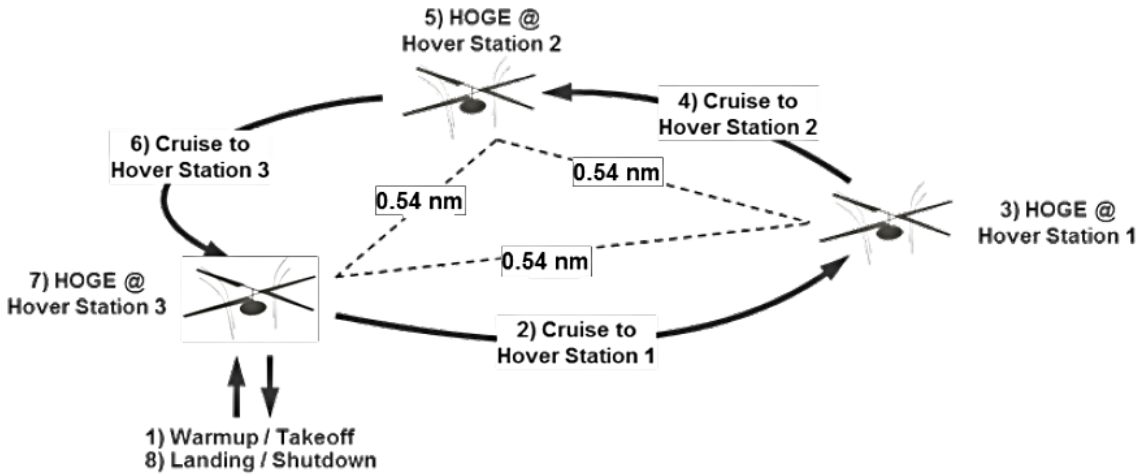

Figure 2.1 24-Hour challenge mission profile.

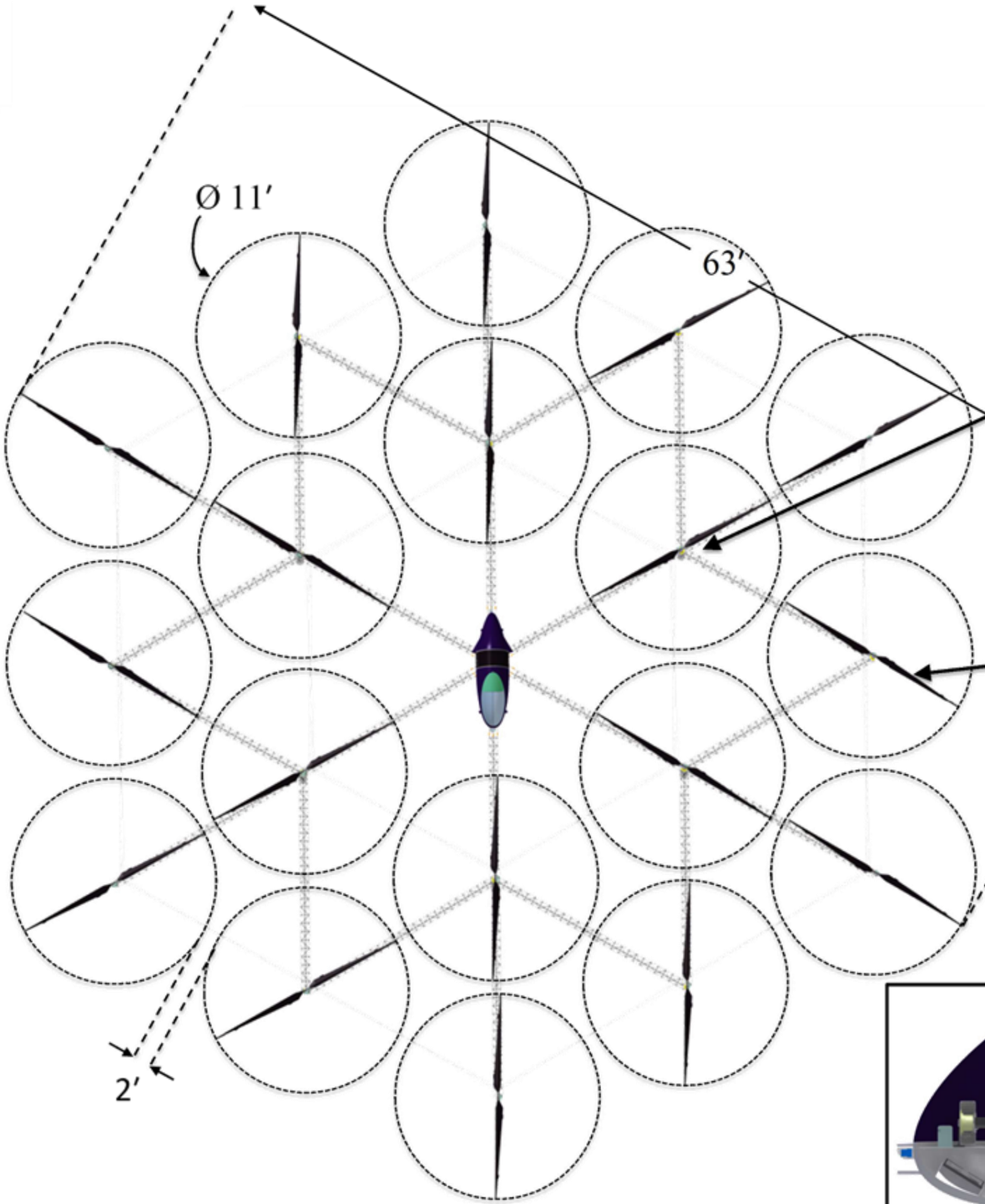

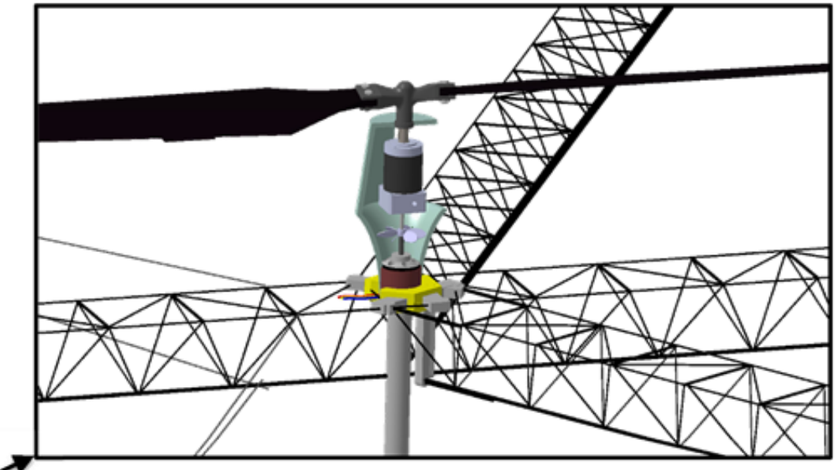

Hub design promotes airflow for cooling through integrated fan, as well as maintaining fixed pitch for rotors.

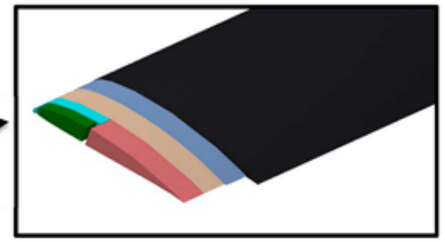

Blade structures designed for weight reduction, as well as aeromechanic considerations.

Fuselage contains payload, main engine and generator, fuel tank, cooling systems, as well as most of craft's avionics package.

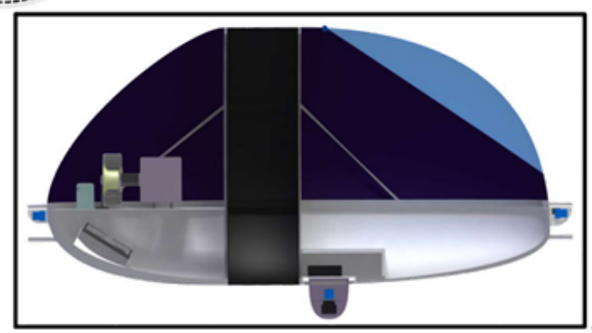

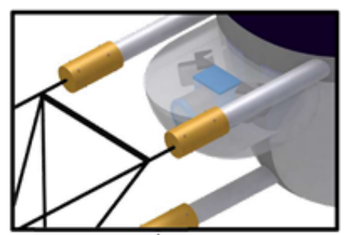

Microtruss structure supports fuselage through three pinned connections at all six connection nodes. This allows for structural integrity as well as modularity and transportability.

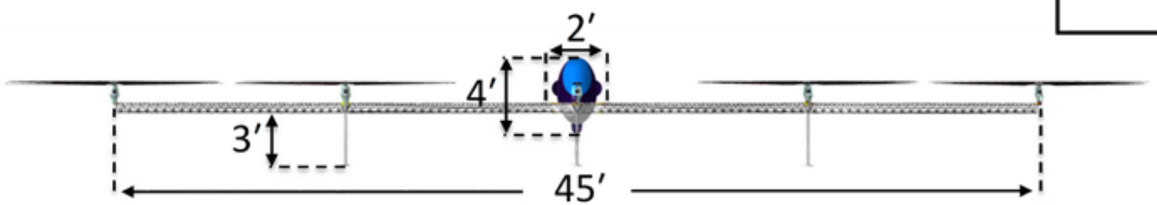

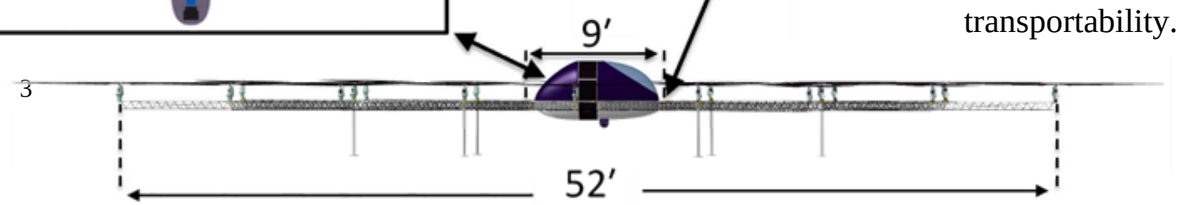

As defined in the RFP, hover is “a condition when the aircraft is supported exclusively by aerodynamic forces, has zero relative velocity with respect to a ground observer station, both longitudinally and laterally, and has no change in altitude. Furthermore, hover shall be defined as out-of-ground-effect (OGE) at an altitude at least twice the largest vehicle dimension. Lastly, hover shall be defined as flight time during which wind speeds do not exceed 9.71 kt (5 m/s).” [35] Additionally, hover time is begun by the aircraft achieving hover within the 65.6 feet (20 m) radius sphere of a Hover Station.

There are two prominent stages required for this mission: forward flight and hover. The vehicle must be able to both hover for the required time and be able to fly efficiently between hover stations. That said, because of the reasonably short distances between hover stations (0.54 nm or 1 km), the vast majority of the mission will be performed while in hover. In addition, the mission must begin and end with controlled climb and controlled descent respectively.

Because hover is defined in the RFP and reaffirmed in the Request for Information (RFI) as zero velocity, the vehicle must also be highly controllable in conditions of less than 9.71 kt (5 m/s) winds. The time spent responding to disturbances is time spent out of hover and therefore wasted fuel.

2.1 Multi-Mission Capabilities/Mission Profiles

Though the basic mission described in the RFP requires hovering for 24 hours between three hover stations with a payload of 80 kg, *Chezoía* is designed to be used for a variety of missions. The entire vehicle is modular which not only allows it to be broken down into smaller parts for easier transport and maintenance, but it also allows the center section to vary in design and purpose. Instead of a pod capable of housing a human, the center section could contain additional cameras for surveillance or inspections, communications equipment to provide or extend the range of cell phone signal, wifi, radio, etc, many other smaller drones, crowd dispersal systems for law enforcement, and any other systems that would gain from having a long-term hovering platform.

Chezoía's capabilities allow it to stay in an area for very long periods of time, but also range wide distances. This can be very useful in disaster situations where searches and rescue can last for days. With additional cameras, *Chezoía* can perform more thorough searches over longer ranges or with more detail. Added thermal cameras could allow *Chezoía* to find survivors under rubble or inside buildings. Similarly, using *Chezoía* as a drone mothership would allow many smaller UAVs to deploy and search many smaller areas. *Chezoía* could also be equipped with an extra battery that could refuel drones who would run out of fuel more quickly than *Chezoía*.

In the unmanned configuration, *Chezoía* can be used to investigate chemical, biological, radiological, nuclear, and explosive hazards. With the addition of certain sensors, multiple aircraft could canvass a large area and take instrument data and visual recordings to survey the site of such a disaster. *Chezoía* could also be used to inspect infrastructure like wind turbines where human inspectors would have difficulty or spend unnecessary time reaching. Drones could be deployed from *Chezoía* to inspect smaller areas or perform minor repairs.

Chezoía could serve as a radio antennae or Wifi hot spot, bringing communication signals to remote places like mountains, deserts, oceans and cities experiencing power outages. *Chezoía* can also be used as a system that can stay on station for long periods of time, waiting to be deployed into action. Should law enforcement expect civil unrest, *Chezoía* can hover nearby with crowd dispersal systems should something break out. Due to its superior controllability, the vehicle could maintain position between buildings within urban streets. *Chezoía* would be capable of using speakers, directed-energy systems, and has a control system capable of handling the recoil of systems with small projectiles

3 Concept of Operations

Chezoía has been designed with ease of use in mind in all aspects of its mission. From transporting the aircraft to its mission site to diagnostic displays for easy maintenance and inspection of electronics and hardware, all aspects of the aircraft's mission cycle have been considered.

3.1 Delivery

Though it has a 2,000 ft^2 (190 m^2) footprint when fully assembled, the aircraft can be delivered in a much smaller assembly kit due to the modularity of its components, as can be seen in Figure 3.1. All components of the aircraft can be shipped inside of two separate delivery crates. The first crate is 9 ft x 2 ft x 4 ft (2.75 m x 0.6 m x 1.2 m), weighs 228.16 lbs (103.49 kg), and contains the entire fuselage section. The second is 13 ft x 2.5 ft x 2.5 ft (3.96 m x 0.76 m x 0.76 m), weighs 373.76 lbs (169.53 kg), and contains the disassembled structure, hubs, rotors, and landing gear. This assembly kit fits entirely inside of a 15 foot (4.5 m) U-Haul truck, four kits can be loaded in a Chinook, as well as four inside a standard 20 foot (6.0 m) shipping container. *Chezoía's* modular design allows for this ease of transportation, as well as facilitating the assembly once the aircraft arrives on location. Additionally, this allows for easy and less costly storage, allowing the craft to be stored in a standard 5 ft x 15 ft (1.5 m x 4.5 m) Public Storage unit, rather than paying for the cost of hanger space.

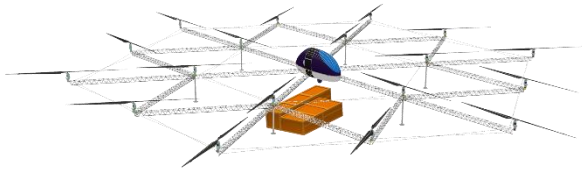

Figure 3.1: Assembly Kit Size.

3.2 Mission Preparation

To load payloads, the front window of the fuselage is on a top hinge, allowing for easy access as can be seen in Figure 3.2. Once inside, the payload area has enough room to accommodate a human pilot, or other payload of equivalent 176.4 lb (80 kg) weight. Loading into this area is carried out at a height of about 5 feet (1.5 m) off the ground. Therefore, entering and loading the vehicle is completed using a portable step platform such as the one pictured in Figure 3.3.

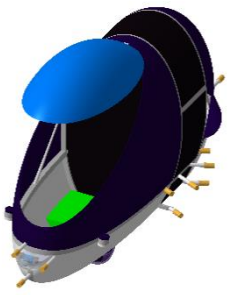

Figure 3.2: Fuselage Payload Hatch.

Additionally, fueling of the aircraft is also completed with the assistance of a step platform, as well as a fuel bowser as shown in Figure 3.3. Fuel is loaded into the tank from the top of the fuselage, which is a total of 7 feet (2.1 m) from the ground. Using a four foot platform as pictured allows for both easy payload and fuel loading.

Chezoía's included startup battery allows for over half an hour of diagnostic checks for the avionics package, prior to the start of the mission. During this time, diagnostic information from all components of the package can be viewed on a GUI located on the bottom of the fuselage, viewable from below. Additionally, this startup battery powers *Chezoía*'s remote starting capability, through the included telemetry unit. With fully autonomous flight, remote startup is the last necessary human involvement in the completion of the mission.

Figure 3.3: Mission Preparation Equipment.

3.3 Service Area

With a service range of over 700 nm (1300 km), *Chezoía* is capable of reaching great distances during flight time. Along with this, it is important that the aircraft also be able to handle a wide range of conditions throughout its flight. With the cooling systems described in Section 9.3, *Chezoía's* systems can operate in ambient temperatures of over 100 °F (37.78 °C). Additionally the aircraft's control scheme allow it to maintain hover in wind speeds of over 35 knots (18 m/s) or at altitudes of up to 7,000 ft (2100 m). Overall, the robust systems included in the design allow for the completion of missions in adverse conditions, allowing for greater overall productivity.

4 Vehicle Configuration Selection

After reviewing the RFP, a number of vehicle configurations were explored and compared for their capabilities for completion of the given mission. These configurations included conventional single main rotor, coaxial, tandem, synchropter, multirotor, cyclocopter, ducted fan, and octo-coaxial designs, displayed in Figure 4.1. Each of these configurations was evaluated based on the design drivers enumerated and explained below. The configurations were then qualitatively compared and ranked through multiple Pugh decision matrices in order to determine the optimal configurations.

4.1 Selection Criteria: Voice of the Customer

The RFP outlines the mission which is to be achieved: the vehicle submitted is required to be capable of 24 hours of continuous hover after takeoff. Hover has been further defined as occurring out-of-ground-effect with a minimum altitude of at least twice the largest vehicle dimension. The 24 hours of hover will be divided between three separate "hover stations" which are imaginary spheres of radius 65.6 feet (20 m), located no less than 0.54 nautical miles (1 km) away from each other. The vehicle must fly with a non-productive payload of at least 176.4 pounds (80 kg); this payload may not aid in providing lift, control, or structural support for the

aircraft. The aircraft will not have any occupants and therefore will need to be flown either autonomously or remotely from a ground controller. The timeline for design, build, and testing of the vehicle must be within the next 3-5 years.

Figure 4.1: Configurations considered, Octo-Coaxial not pictured.

Additionally, the RFP outlines several strategies that cannot be utilized by the aircraft. The aircraft cannot collect energy from sources outside of the aircraft, with exceptions for uses in flight control and telemetry communication, as well as the collection of solar irradiation and atmospheric gases for combustion or electrolysis. The aircraft is also restricted from trapping lighter-than-air gasses and all of the closed cavities must be vented to the atmosphere. Throughout the course of its mission, no part of the vehicle is permitted to be jettisoned for any reason during flight.

In addition to the requirements explicitly stated in the RFP, considerations were added by the team with the goal of optimizing customer satisfaction with the final product. These included the cost of the vehicle, its practicality, and safety, as well as considerations for public relations and acceptance of the proposed aircraft.

From both the explicit and implicit requirements set forth for the designed vehicle, over 50 specific design criteria were considered for use in evaluating possible designs. These criteria were compiled based on specific requirements outlined in the RFP as well as other criteria generated by the team. From this initial listing, the focus was narrowed based on the mission relevance and relative importance of each criterion to the success of the mission. Through these considerations, the initial criteria were integrated or eliminated until a consensus was reached on the 10 most important design drivers. These are listed and defined below alongside their relevant RFP requirements in Figure 4.2. As can be seen, each of the design drivers was derived directly from the explicit and implicit voice of the customer requirements listed in the RFP.

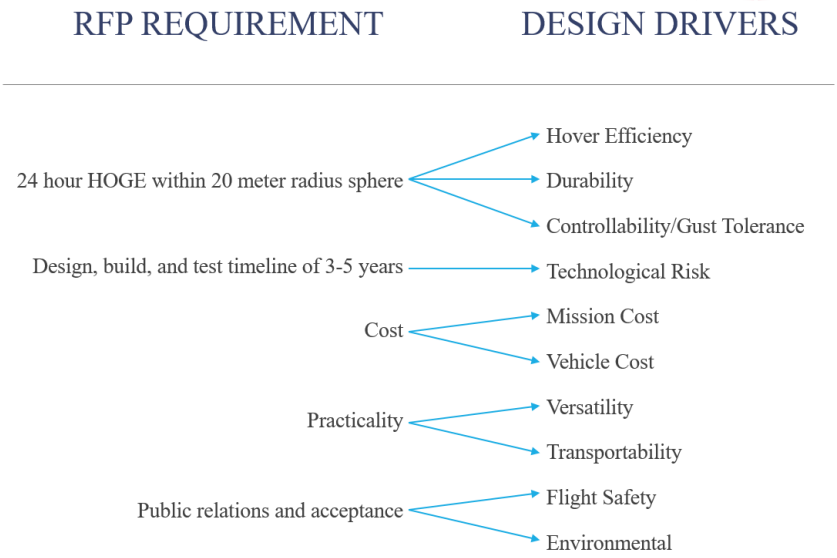

Figure 4.2: Development of selection criteria.

Hover Efficiency: Because of the driving focus on hover during the mission, the aircraft needs the ability to hover with the least power necessary, throughout the full duration of the mission. This criterion takes into consideration the power and fuel required for the mission of 24 hour hover. A large part of evaluating these criteria was completed through analysis of the sizing code described in Section 5.2.

Durability: To complete the mission, the chosen configuration must be able to operate continuously for at least 25 hours with no maintenance. This criterion is a measure of each configuration's ability for the entire assembly to withstand the extended flight time. This takes into account factors such as mechanical complexity, redundancy, and changes in operating conditions.

Controllability and Gust Tolerance: The aircraft is required to hover within a 65.6 feet (20 m) radius sphere, allowing for winds up to 9.71 kt (5 m/s), while maintaining zero velocity relative to the ground. Additionally, it must climb, fly between stations, and descend in a similarly controlled manner as well. This will require every configuration to have robust control systems, especially in hover, to meet this requirement.

Technological Risk: The timeline provided for the design, build, and testing of the aircraft is the next 3-5 years. This requires that any technologies or developments necessary for the design must either be available or fully developable within that short span. This is defined as a measure of the availability and confidence in the technologies which are necessary for the success of any given configuration.

Mission Cost: There will be significant monetary cost associated with every flight of the aircraft, due to the large amounts of fuel required for each. This criterion is the qualitative cost of each 25 hour flight for any given configuration. A major factor in this cost is the amount of fuel necessary, but also includes expected maintenance and repairs.

Vehicle Cost: Aircraft are expensive to develop and manufacture. This is a qualitative measure of the lump sum cost of the chosen configuration. This includes the cost of parts and labor, as well as considerations for the complexity of design and decommissioning at the end of the aircraft's lifecycle.

Versatility: A successful configuration should also have capabilities which can extend to a variety of applications for an extended hover machine. This measures the ability of a configuration to complete related missions, including considerations for forward flight, range, and changes in operating conditions.

Transportability: The manner in which the aircraft will arrive at the site of the mission should be taken into consideration for practicality. Based on the University of Maryland's experience with *Gamera*, a vehicle with a large footprint tends to be more efficient, but also more difficult to set up and move. This criterion is a qualitative measure of the ease of transporting a given configuration, including the configuration's ground footprint and potential for breaking down into subassemblies and reassembling the machine on site.

Flight Safety: Although this is an unmanned mission, safety must always be taken into consideration. There will be substantial resources invested in the development and flight of the vehicle, so it is important that dangers to the vehicle and those around it are minimized for the protection of the machine as well as the immediate mission area. This criterion is a measure of the qualitative risks associated with the flight and possible in-flight issues during the mission.

Environmental: This mission is expected to be completed within a relatively small area, though it will last for an extended period of time. With this in mind, the design should attempt to minimize disruptions or adverse effects of its operation on people or things that are within or near the mission area. This criteria qualifies the effects of the configuration's operation, including acoustics and potential greenhouse gases produced.

4.2 Selection Criteria: Analytical Hierarchy Process

Following the development of the selection criteria, relative weightings for the importance of each within the scope of the RFP were determined through an Analytical Hierarchy Process (AHP) [1]. This facilitated the prioritization of criteria as more important to the mission over those which are not mission critical. For this process each member of the team individually filled out a relative importance matrix, comparing every criteria with each other on a scale from less important (< 1.0), or more important (> 1.0). Columns were then normalized and each criteria's score across rows was averaged to attain relative weightings for each criteria.

After each member completed this process the team came together to discuss individual considerations and findings. Following multiple iterations of discussion and adjustments, a consensus was reached for the weightings of the selection criteria, which can be seen below in

Table 4.1. This Analytical Hierarchy Matrix was used to qualitatively weight the importance of each selection criterion. The matrix is read as relative importance of each horizontal row against each vertical column. For example, the '4' in the Hovering Efficiency row signifies that Hovering Efficiency was determined to be roughly four times as important as Controllability. From these raw scores, weightings were determined by summing and normalizing each row. With this consensus, it was clear that hovering efficiency, durability, and controllability were the most mission critical elements, though versatility, transportability, and mission cost also became top design drivers. The other criteria, though important to consider, were weighted considerably lower than the aforementioned top criteria.

Table 4.1: Analytical Hierarchy Matrix used to weight the importance of selection criterion.

	Hovering Efficiency	Durability	Controlability	Versatility	Mission Cost	Transportability	Vehicle Cost	Flight Safety	Technological Risk	Environmental	Weight
Hovering Efficiency	1	1	4	3	6	3	6	8	5	8	0.25
Durability	1	1	4	2	7	3	7	7	4	9	0.24
Controlability	0.25	0.25	1	1	5	2	6	4	4	7	0.13
Versatility	0.33	0.5	1	1	3	2	4	6	5	5	0.13
Mission Cost	0.17	0.14	0.2	0.33	1	1	2	0.5	3	4	0.05
Transportability	0.33	0.33	0.5	0.5	1	1	2	2	4	4	0.07
Vehicle Cost	0.17	0.14	0.17	0.25	0.5	0.5	1	0.33	0.5	3	0.03
Flight Safety	0.13	0.14	0.25	0.17	2	0.5	3	1	1	3	0.04
Technological Risk	0.2	0.25	0.25	0.2	0.33	0.25	2	1	1	2	0.04
Environmental	0.13	0.11	0.14	0.2	0.25	0.25	0.33	0.33	0.5	1	0.02

4.3 Considered Configurations

Many configurations were considered for completion of the 24 hour hover mission outlined in the RFP. Below, each configuration is listed and discussed on a high level in terms of its advantages and disadvantages. Due to the nature of the mission, forward flight characteristics were considered significantly less important than hovering and control characteristics. Top designs require inherent stability, high hovering efficiency, and robustness to complete the entire mission.

Single Main Rotor: Single main rotor (SMR) configurations are the most common helicopters. They are well balanced in terms of our criteria and so was used as a baseline. The single rotor and hub make the system simple while having good hovering efficiency; however, a tail rotor is required for anti-torque which uses about ten percent of the total available power.

Coaxial: A coaxial configuration is similar to a SMR configuration, however it does not require the extra weight and power for a tail rotor and involves a more complex hub. Its merits in hover compared to SMR depend on how you define disk loading.

Cyclocopter: This mostly experimental helicopter configuration has been shown to potentially have greater hovering efficiency than a SMR and its superiority in forward flight make it a very versatile configuration [2]. However, they have only been built in small scale and there are many uncertainties associated with the aerodynamic and structural properties at the scale required for the mission.

Ducted Fan: A ducted configuration has increased hovering efficiency over a non-ducted system and provides protection for the rotors. However, this would be heavier than an open rotor system,

and would be viable only if the increase in thrust is more than the increase in weight. Additional structure would also make the configuration more susceptible to wind gusts.

Multirotor: We have defined multirotor as a helicopter with a symmetrical distribution of three or more rotors around a center section. Multirotor systems are the simplest configuration to control because it uses RPM manipulation which is easy to implement. On a full scale vehicle, collective and cyclic controls may be added for increased control. The larger number of rotors, though mechanically simpler, require additional support structure.

Octorotor Coaxial: This configuration was considered in order to take advantage of both a multirotor's stability and a coaxial's hovering efficiency.

Tandem: Tandem configurations require less power on each rotor and a SMR of equivalent disk loading and do not require a tail rotor for anti-torque. It has a better power loading to a coaxial of equivalent disk loading but has a larger footprint which helps maintain stability by allowing a greater range of movement of the CG.

Synchropter: Synchropter configurations are characterized by a dual hub design with intermeshing rotors, combining characteristics of tandem and coaxial designs, leading to strong performance in hover as well as having excellent stability and control. Historically, they have often been used as heavy lift and cargo transport vehicles.

4.4 Pugh Decision Matrix

The Pugh decision process was utilized to generate quantitative rankings of the above configurations. Using the selection criteria described in section 4.1 and the relative weightings of these criteria developed through the Analytical Hierarchy Process, the configurations were assessed for relative effectiveness with each criterion. As can be seen in Table 4.2, each configuration was given a relative score for each selection criteria and the scores were then weighted and summed across each configuration to compare overall performance characteristics. Single main rotor was used as the base configuration and each configuration was judged for each criteria as either better or worse than SMR for individual criterion. The highest total scores are reflective of configurations more suited for the mission profile. Through this process, it was clear that the multirotor, synchropter, and tandem designs were superior to the others, with the multirotor as the leading configuration.

Table 4.2: Pugh Matrix used to evaluate each configuration across all selection criteria.

Wt.	Design Criteria	SMR	Coax	Tandem	Multirotor	Cyclocopter	Ducted	Octo-coax	Synchrocopter
0.25	Hovering Efficiency	0	2	2	2	4	2	2	3
0.24	Durability	0	-2	0	2	-6	0	-4	-1
0.13	Controlability	0	-2	-2	0	-2	-4	0	2
0.13	Versatility	0	2	2	2	-4	0	0	-2
0.05	Mission Cost	0	2	2	2	4	0	2	3
0.07	Transportability	0	2	2	4	2	-2	2	2
0.03	Vehicle Cost	0	-2	0	0	-4	-2	-4	0
0.04	Flight Safety	0	2	4	4	-4	4	-2	2
0.04	Technological Risk	0	-2	0	0	-6	-2	-4	0
0.02	Environmental	0	2	2	2	2	2	0	2
	Total	0.00	0.24	0.94	1.82	-1.36	-0.10	-0.58	0.92

Due to the requirements of the mission, several configurations were not considered during this process. These mainly consisted of configurations which perform well in forward flight rather than in hover. For this reason, no form of autogyro was considered since it is not capable of pure hover. Additionally, no compound or fixed wing designs were considered because of their heavy emphasis on forward flight compared to hover. For similar reasons, no tilt rotor designs were explored in detail either.

5 Preliminary Vehicle Sizing

An in-house sizing algorithm based on the methodology of Tishchenko [3] was developed to estimate the weight, dimensions, and power requirements of a variety of vehicle configurations. A variety of estimates for weights and performance were used including the Army's Aero Flight Dynamics Directorate (AFDD) empty weight model for rotors and hubs used in NDARC [4], in-house models for the unique structural considerations of the vehicle, and estimates for the power and energy density of motors and power sources [5]. This section will describe the assumptions of the sizing algorithm and present the results of a set of trade studies that led to the selection of the vehicle's rotor configuration, engine, and other performance parameters.

5.1 Sizing Mission

The mission profile for *Chezoía* is dominated by hovering flight. Based on the RFP specifications, the mission input into the sizing code was to hover for 25 hours, with the extra hour to account for disturbances when the wind speed exceeded 9.71 knots (5 m/s). Since flight at 30 knots (15.4 m/s) would mean that the total forward flight time for the vehicle is less than 2 minutes (less than 0.2% of a 25 hr mission time) and the time to climb at least 2 vehicle dimensions is of a similar time required, those components of the mission were left out of the sizing code because they would have an insignificant impact on the results of the preliminary sizing. The vehicle was also required to carry the 176.4 lb (80 kg) payload, and 100 lb (45.4 kg) of electronics weight. The mission was assumed to take place at sea level density because this would lead to the best engine performance. The engines were sized to be able to provide 10% more thrust than required in hover for takeoff performance and required control inputs.

5.2 Sizing Methodology

Chezoía's sizing algorithm was based on an iterative procedure using the basic Tishchenko methodology for rotorcraft sizing. Along with the RFP mission profile, the sizing method is initialized by a set of inputs, which were iterated upon to determine the vehicle's gross takeoff weight (GTOW). The set of inputs are varied and used to determine the ideal design parameters for the vehicle.

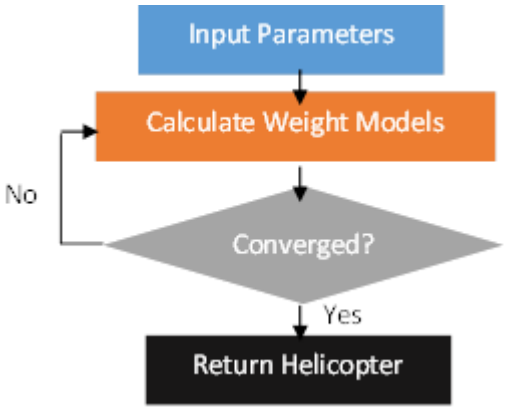

Figure 5.1: Basic sizing methodology algorithm.

The sizing algorithm is organized as follows:

1. The mission and vehicle parameters are input into the program. The inputs include configuration

type, engine type, number of blades per rotor, blade aspect ratio, blade loading, rotor tip speed, and Figure of Merit (FM) are input. A relatively low FM is used throughout the preliminary sizing to allow for potential underestimates in the weight of the structure and auxiliary components. An initial guess weight is input as well.

2. The following steps are iterated until the value for GTOW converges:
    a. The rotor chord and diameter, as well as the disk loading, is calculated from the blades per rotor, blade loading, aspect ratio, and tip speed.
    b. AFDD models are used to calculate the rotor hub and shaft weights.
    c. The in-house structural model, and transmission model (when not using an electric or hybrid system) are used to calculate structural weights.
    d. Engine power-to-weight ratios are used to calculate the propulsion system weight.
    e. Fuel weight for the complete mission is calculated using the fuel energy density, engine density, and FM. For ease of comparison, the FM was assumed to remain constant throughout the mission. Additionally, this assumption is true for a rotor which uses tip speed to vary the thrust.
3. The final helicopter parameters calculated in step 2 are returned.

The sizing program was validated against the plots produced in the RFP, and the resulting outputs provided a very close match. An example comparison can be seen in Figure 5.2.

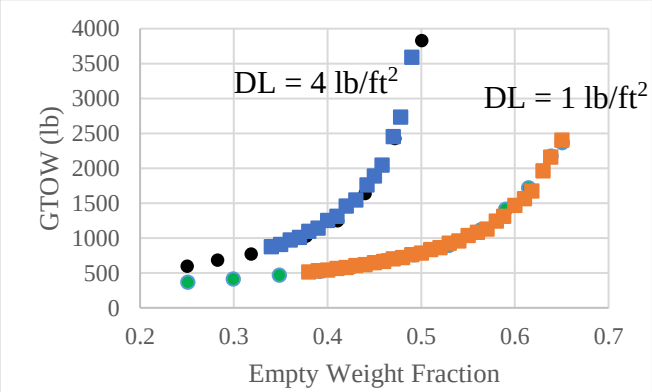

Figure 5.2: Comparison of data provided in the RFP (circles) and data output by the sizing code (squares).

5.3 Multirotor and Engine System Selection

Selection of the number of rotors and engine system are interconnected. For this reason, the results of the sizing program for engines and multirotor type configuration are presented together.

A variety of multirotor configurations were included in the program to analyze a wide range of potential multirotors. Since the tandem rotor configuration could also be treated as a multirotor, it was also included in this analysis. The multirotors consisted of 2, 4, 8, 16, 18, and 20 rotor configurations.

The engine systems considered in the sizing program are:

- Turbine
- Gasoline
- Diesel
- Fuel cell electric
- Battery electric
- Turbine-electric hybrid
- Diesel-electric hybrid

Each engine and fuel system had a corresponding power-to-weight ratio, energy density, and conversion efficiency. The fuel-cell system also had the weight of its entire stack, including the pressurized fuel tank, accounted for. The hybrid systems are assumed to have an 85% engine shaft to rotor shaft conversion efficiency.

Since the layouts of the different multirotors varied widely, the ideal engine selection for a given configuration was expected to be different for different multirotors. It was hypothesized that configurations such as Tandem layouts would perform better with physical transmissions, but the complex layout of higher numbers of rotors (16, 18, and 20) would perform better with hybrid systems with electric transmissions. This hypothesis was confirmed by the sizing program.

Figure 5.3.a shows a comparison of a Tandem and 18-rotor configuration. The battery electric and fuel-cell electric engine systems did not yield a converged solution, because the energy density is very low for these systems. Additionally, the gasoline engine is not shown for the 18-rotor, because the weight of the transmission and inefficient nature of the engine cause it to not converge. The Tandem configuration has its lowest GTOW with a turbine engine, and the 18-rotor with a turbine-electric hybrid.

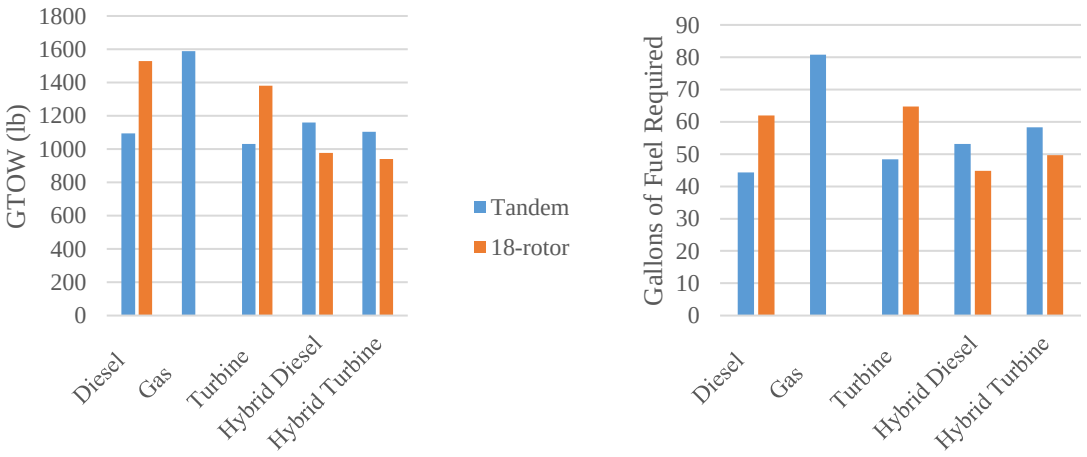

(a) Takeoff weight *(b) Fuel used*

Figure 5.3: Comparison of the Tandem and 18-rotor configurations with varying engine configurations. Held constant are the FM (0.62), disk loading (0.81 lb/ft^2), blade loading (0.12), number of blades (2), and blade aspect ratio (20).

GTOW was not the only consideration in selecting an engine system. The amount of fuel used is important in determining the overall system efficiency. Shown in Figure 5.3.b is the total amount of fuel used for the hover mission by the Tandem and 18-rotor with each engine configuration. The Tandem, diesel-engine and 18-rotor, diesel-hybrid-engine configurations are the lowest and use approximately the same amount of fuel. Even though the turbine-electric hybrid configurations are lighter, the diesel-electric hybrid versions use less fuel for the mission.

Based on these results, the diesel-hybrid was chosen both because it offered lower fuel consumption than other non-diesel engines, and because the hybrid allows a variety of other

benefits. The hybrid engine allows for variable speed electric motors to control thrust through tip speed, and for a backup battery to allow for redundancy.

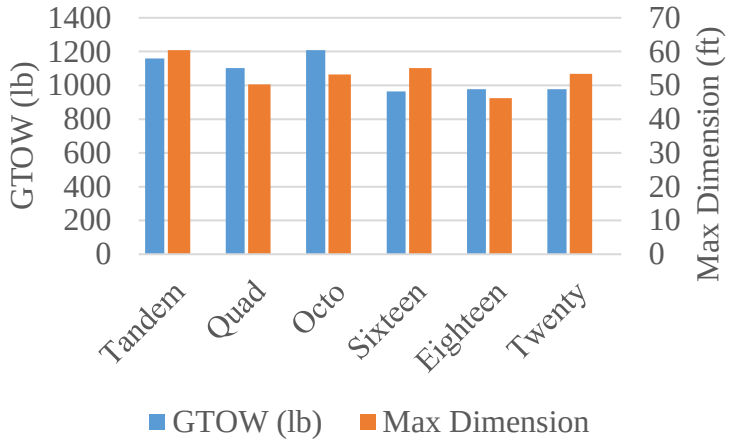

Figure 5.4: Comparison of take-off weights of different multirotor configurations with a diesel-hybrid engine. Held constant are FM (0.62), disk loading (0.81 lb/ft^2), blade loading (0.12), number of blades (2), and blade aspect ratio (20).

The results of the diesel-hybrid engine fitted on the other rotor configurations are shown in Figure 5.4. Of the configurations with less than 10 rotors, the Quadcopter has the lowest GTOW, and it has the smallest footprint. However, the three configurations analyzed with more than 10 rotors have takeoff weights lower than those in the "less than 10 rotor" group. Using a large number of rotors is also ideal for the hover mission because the vehicle can operate with one or more rotors inoperative if required. A large number of rotors allows some motors to be turned off for cooling, while the other rotors absorb the slightly higher thrust requirement due to a motor being turned off. Based off the sizing results, the weight of all the high rotor number configurations was comparable. The 18-rotor configuration was ultimately chosen because it provided a large central section outside of the downwash of any of the rotors for the hub, and the maximum dimension was slightly smaller than the 16 and 20 rotor configurations. The 18-rotor configuration was also longitudinally and laterally symmetric and allowed for the adaption of existing, proven control schemes.

5.4 Trade Studies

5.4.1 Disk Loading and Hover Tip Speed

Disk loading is one of the most important parameters to optimize for efficient hover. While disk loading was not a direct input into the program, it could be manipulated by changing the input tip speed of the rotor, assuming a constant blade loading.

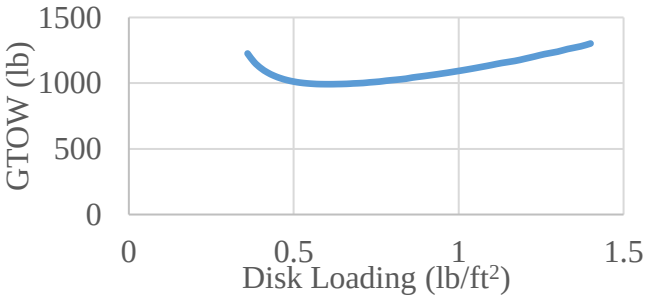

Figure 5.5: Varying disk loading for 18-rotor diesel hybrid configuration reveals disk loading with minimum take-off weight. Held constant are FM (0.62), blade loading (0.12), number of blades (2), and blade aspect ratio (20).

Through a sweep of tip speeds, a minimum GTOW occurred at a disk loading of 0.61 lb/ft^2, as can be seen in Figure 5.5. This disk loading corresponds with a tip speed of 260 ft/s (79.2 m/s). This disk loading may seem low when compared to other light helicopters such as the Robinson R22 [6], which has a disk loading of 2.6 lb/ft^2, but is larger than that of other low powered helicopters such as *Gamera*, which has a disk loading of approximately 0.03 lb/ft^2 [7].

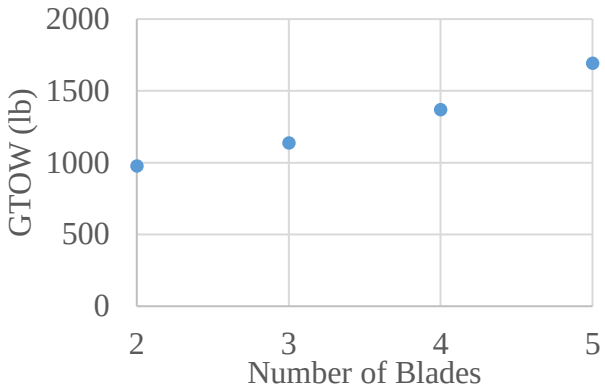

Figure 5.6: Increasing number of blades per rotor for 18-rotor diesel hybrid increases weight. Held constant are FM (0.62), blade loading (0.12), number of blades (2), and blade aspect ratio (20).

5.4.2 Number of Blades

The number of blades per rotor was also a big factor in the GTOW of the vehicle. Increasing the number of blades monotonically increased the GTOW of the vehicle, as can be seen in Figure 5.6. Using one blade per rotor was not considered because of the need for a non-productive counter weight to balance the rotor.

5.5 Results of Preliminary Sizing

The parameters of the design resulting from the sizing code can be seen in Table 5.1. These parameters were fixed throughout the design. Some of the parameters used in the sizing code, such as FM, are not presented here because they were underestimates and were calculated more precisely in detailed design.

Table 5.1: The sizing parameters used to design Chezoía.

Parameter	Value
Number of Rotors	18
Engine Configuration	Diesel-electric hybrid
GTOW	1010 lb (458.1 kg)
Rotor Radius	5.5 ft (1.68 m)
Disk Loading	0.6 lb/ft^2 (28.73 N/m^2)
Rotor Tip Speed	260 ft/s (79.2 m/s)
Blades per Rotor	2

6 Rotor Design

Hover performance was the prime driver for the design of the rotor system. Developing a rotor system which had high power loading was integral to the success of the *Chezoía* design. As the configuration selection resulted in the selection of many small rotors with relatively low tip speed, the design aims to make use of innovation in low Reynolds number aerodynamics and field-proven lightweight, low-cost structural design. It is necessary for each of the 18 rotors to provide 56 lb (249 N) of thrust while using as little power as possible.

Figure 6.1: Rotor side view.

6.1 Rotor Aerodynamic Design

6.1.1 Airfoil Selection

The process of developing the rotor design began with the selection of the airfoil or airfoils. The sizing selection process dictated that a tip speed of 260 ft/s (79.2 m/s) and an aspect ratio of around 20 would be ideal, and a baseline tip Reynolds number of 400,000 was determined. This relatively low Reynolds number meant that airfoil technology used for traditional helicopters may not be ideal for the *Chezoía* rotor.

A large variety of airfoils were considered to provide ideal hovering performance for the rotor. To analyze the airfoil properties, XFOIL, using a free transition model, was used to generate lookup tables of lift, drag, and moment coefficients [8]. The XFOIL results for a select group of airfoils is presented in Figure 6.3. When available, these results were compared with experimental data.

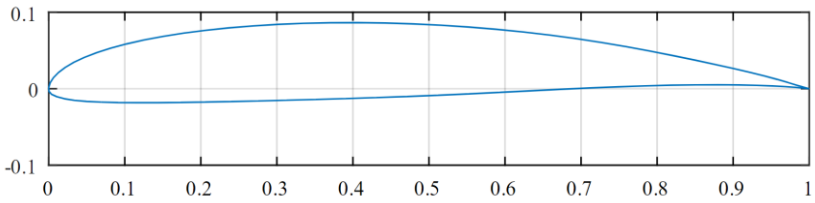

Figure 6.2: Selected SG6042 airfoil geometry

The NACA0012 was chosen as a baseline because of its well-studied performance. However, its lift-to-drag ratio is inferior to second- and third- generation airfoils. The NACA23012 showed improved lift-to-drag performance and peak lift coefficient over the NACA0012. Proprietary airfoils such as Sikorsky's 36212 [9] and Boeing's VR5 can further improve lift-to-drag. One drawback of the VR5 is the sharp peak in L/D, which means that complex twist shapes may be necessary to ensure efficient operation. These two airfoils also have limited published experimental data for force coefficients below Reynolds numbers of 400,000.

All of the previously mentioned airfoils have been used successfully in current helicopter designs. However, the low Reynolds number design necessitated the use of a more tailored airfoil. The SG60XX series of airfoils were designed for ideal lift-to-drag performance at a Reynolds number of 300,000. The SG6041, SG6042, and SG6043 (in increasing order of camber) show good performance in this Reynolds number regime, and as can be seen in Figure 6.3, the SG6042, pictured in Figure 6.2 strongly outperforms the other airfoils in both lift-to-drag ratio and peak lift coefficient. The presented peak lift-to-drag and peak lift coefficient predicted by XFOIL show good correlation with experimental data as well [10]. A comparison of XFOIL data to experimental data can be seen in Figure 6.4. This series of airfoils has a slightly larger pitching moment coefficient than the other presented airfoils, but the lower dynamic pressure than typical helicopter rotors afforded by the lower tip speed means the torsional stiffness is less of a concern. The SG6042 was ultimately chosen to be the primary airfoil from this set of airfoils because it represented a balance of lift-to-drag performance and moment coefficient.

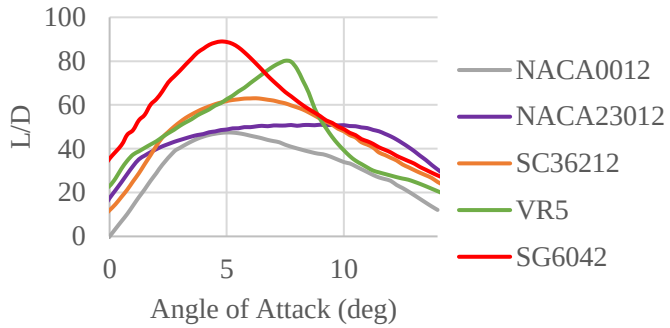

(a) Lift-over-drag

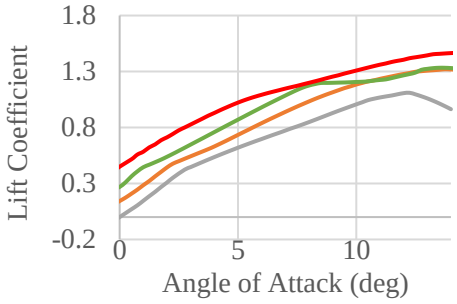

(b) Lift

Figure 6.3: Airfoil characteristics from XFOIL.

The use of a secondary, in-board airfoil, such as one with reflex camber to enable the reduction of the torsional moment, was considered. However, after an optimized single airfoil rotor design was developed, the use of different airfoils was determined to have more manufacturing penalties than benefits to the aerodynamic design.

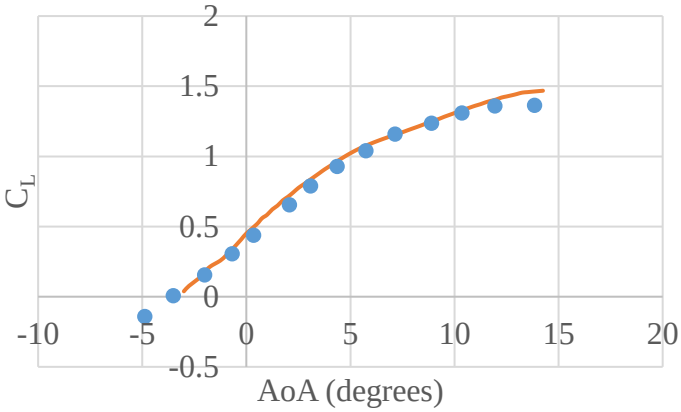

Figure 6.4: Experimental data [34] (dots) and XFOIL data (line) comparison for the SG6042 at a Reynolds number of 200,000 and free turbulence transition.

6.1.2 Twist and Taper Distribution

A Blade Element Momentum Theory code developed by the team was the primary tool used for analysis of the rotor design. The code incorporated tip loss effects, as well as airfoil table lookup based on angle of attack and Reynolds number. These tables were populated with data generated in XFOIL. Since the tip Mach number was well below 0.3, the aerodynamic properties would not vary widely with Mach number so the incompressible limit of zero Mach number was used for extracting lift and drag coefficients.

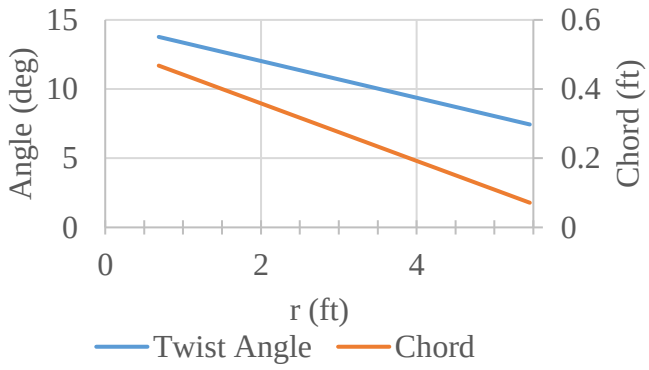

Figure 6.5: The twist angle and chord for the final blade as a function of radius.

To provide a baseline for the design optimization, a straight blade with an aspect ratio of 20 and linear twist of 5

degrees was analyzed. This design provided a power loading of 36.2 lb/hp (0.216 N/W) at the desired hover thrust of 56 lb (249 N) per rotor.

Design optimization was achieved through a sweep of design variables. The first step to moving beyond the constant chord design was a linear twist and taper design. The two equations for twist and taper could each be parameterized by two variables, for a total of four variables. The design sweep was constrained by the 56 lb (249 N) thrust per rotor requirement and the objective was to minimize the power in hover.

Table 6.1: Aerodynamic properties of the rotor.

Rotor Parameter	Value
C_T	0.0037
C_P	$1.96 \cdot 10^{-4}$
FM	0.803
K (induced power factor)	1.0475
Taper Ratio	0.144
Twist (Root to Tip)	6.39°
AR	20.5
C_T/σ	0.175

The resulting blade has a power loading of 39.7 lb/hp (0.237 N/W). The resulting twist and taper distribution can be seen in Figure 6.5. The inflow as a function of the radial position, and the angle of attack distribution can be seen in Figure 6.6. From this figure, it can be seen that over most of the blade the angle of attack is within the range of 4 to 6 degrees, where the highest L/D for the SG6042 airfoil occurs. Since the region not within the ideal lift-to-drag angle of attacks is within the 20% inboard section, which corresponds with less than 5% of area, it was determined that moving to bi-linear twist and taper would not provide significant aerodynamic benefits.

The parameters resulting from the design optimization are shown in Table 6.1. Note that the blade loading (C_T/σ) is higher than for typical rotor blades, but the high lift SG6042 airfoil affords higher blade loading before stall. The blade loading corresponds to a C_L of 1.05, well below the peak C_L of 1.47.

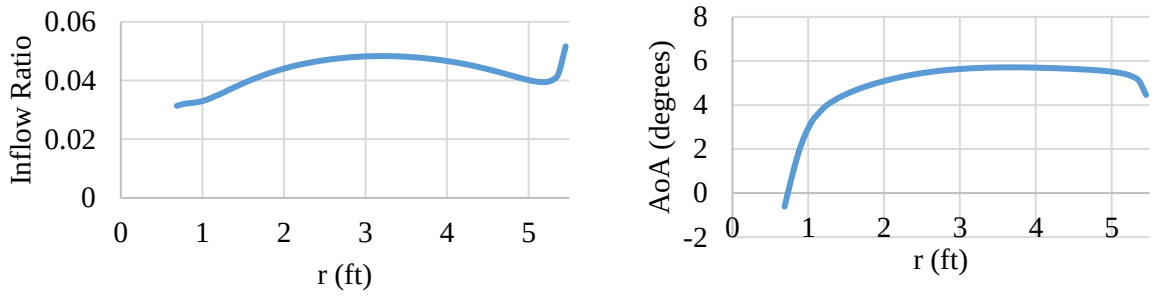

(a) Inflow ratio *(b) Local angle of attack*

Figure 6.6: The induced inflow and resulting angle of attack as a function of radius. The inflow is relatively close to the uniform inflow that is ideal for hover efficiency.

6.1.3 Tip Loss Effects

Tip devices are commonly used to improve aerodynamic performance. Since the rotor design has a low tip speed, the tips are not swept to offset drag divergence. The BEMT code was also run ignoring tip loss effects to analyze the change in power loading when tip loss was included and

when it was ignored. The power loading for the rotor without tip loss effects was approximately 0.5 lb/hp (0.003 N/W) higher. This implies that for the same power, each rotor would produce 0.70 lb more thrust, an increase of 1.5%. The highly tapered nature of the blade and high aspect ratio reduces the penalties of tip loss effects. Even though it would be possible to manufacture small dihedral blade tips at a weight penalty of less than 0.7 lbs (0.32 kg) per rotor, they would likely not eliminate all of the tip loss, and be an additional manufacturing cost. Because the performance increase is marginal, dihedral is not used for the rotor blades.

6.1.4 Additional Rotor Modifications

Each rotor includes a set of fixed-trim tabs, one inboard and one outboard. These trim tabs allow for aerodynamic balancing of the blades, as the fixed hub prevents adjustment of blade pitch after manufacture.

Each rotor also has a 12.5% root cut-out, with a faring on the inboard of the rotor section to reduce drag. The rotor is joined to the hub by two bolts, one on either side of the center of pressure (¼ chord) of the rotor.

The outer rotors are canted inwards at 2º for stability. This reduces the thrust by only 0.07% and so results in a negligible change in hover performance.

6.2 Thrust Variation

The rotor hub is fixed pitch and thrust adjustments are achieved through variation of the rotational speed of the rotor. This constraint means that the figure of merit remains constant at 0.803 throughout the rotor's hover mission and regardless of mission weight. Additionally, since C_T is non-dimensionalized by tip speed and tip speed variations are used to control the rotor thrust, C_T/σ remains constant throughout the mission. However, the power loading varies as the rotor changes rotational speed. The relationship can be seen in Figure 6.7. As the rotational speed decreases within the operating range, the power loading of the rotor increases. This relationship indicates that as the vehicle uses fuel and reduces its tip speed to account for the lower thrust, efficiency is improved.

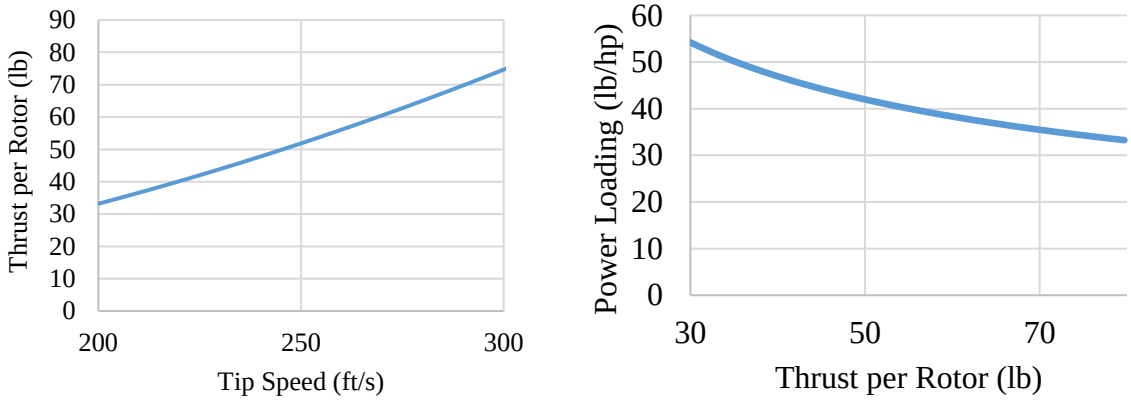

(a) Tip Speed vs. Thrust *(b) Thrust vs. Power Loading*

Figure 6.7: Effects of varying tip speed and resulting thrust.

6.3 Rotor Forward Flight Performance

Since the rotor is designed for high power loading, the L/D_e of the rotors is also higher than typical helicopters such as the UH-60A and CH-47D [11]. The vehicle is limited to an advance ratio of 0.24 which corresponds with a maximum L/D_e of 12.9. The results of the calculation of L/D_e is included in Table 6.2.

Table 6.2: Rotor lift to equivalent rotor drag.

μ	L	D_e	L/D_e
0.05	56.1	42.04	1.33
0.10	56.1	14.84	3.77
0.15	56.1	8.09	6.93
0.20	56.1	5.44	10.3

6.4 Structural Design

The 12.5% radius root cutout consists of an aluminum tube that is pinned into the central rotor hub. From 12.5% span to the tip, the blade has a 6.94:1 taper ratio (from root to tip). The total weight of each blade is 3.89 lb (1.76 kg).

The internal structure of the blades is shown in Figure 6.8. The selection of composite materials in the spar allows the blade to resist high flap and lag moments. The blade is wrapped with layers of ±45º graphite with epoxy to form the skin to maintain the aerodynamic shape and provide torsional stiffness. A D-spar spanning from 2% to 35% chord is constructed with ±45º graphite with epoxy to add flap and lag stiffness at the root of the blade. Nomex honeycomb was chosen as the filler material for the trailing edge section to preserve the shape of the cross section. Care was taken to ensure that the elastic axis of the blade was located at the quarter chord. The center of gravity was aligned with the elastic axis at the quarter chord. A thin copper mesh provides electric bonding to protect the blade form lightning strikes. A stainless-steel strip on the leading edge protects the blade from abrasion and corrosion.

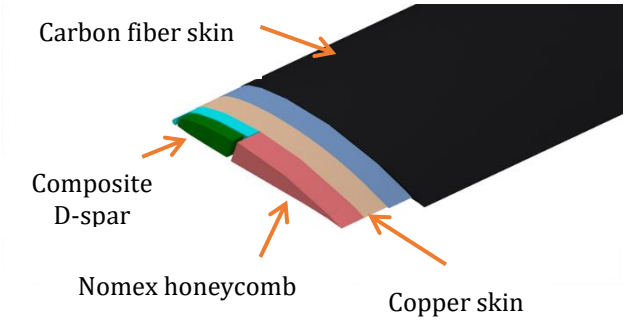

Figure 6.8: Cutaway view of the rotor blade.

6.5 Rotor Blade Cross Sectional Properties

The internal structure of the blade was designed by calculating spanwise blade mass and stiffness properties as a function of airfoil thickness and chord length. Significant parameters considered were airfoil D-spar thickness, D-spar chordwise length, and skin thickness. Spanwise distributions of stiffness, mass, and inertia properties were then used as inputs in Dymore to calculate the first five blade vibratory modes. The flap and lag stiffness at the root were chosen to ensure the stresses experienced do not exceed the allowable limits on the spar.

6.6 Rotor Stability & Blade Stress Analysis

Aeroelastic instabilities from pitch-flap coupling, pitch divergence, and flap-lag coupling were considered in the design of the internal blade structure. The fan plot for one of *Chezoía*'s blades is shown in Figure 6.9. *Chezoía*'s rotors are hingeless, and stiff in-plane, and the fan plot shows that the rotor does not experience resonance during normal operation. The high torsional frequency ensures that the rotor does not suffer large torsional deformations during operation.

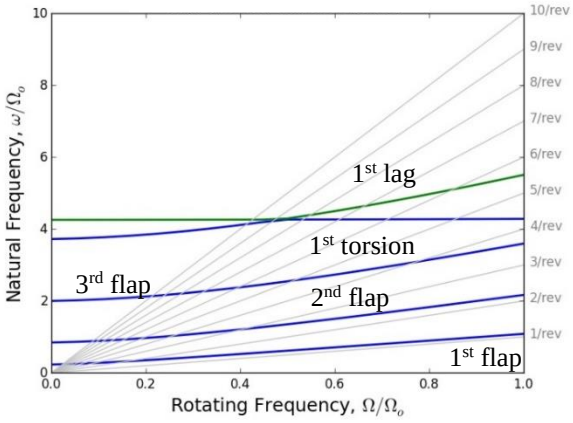

Figure 6.9: Chezoía rotor fan plot.

The rotor blade stresses in hover were predicted using Euler-Bernoulli beam theory. These stresses we found to be less than the maximum allowable stresses of the spar.

The cross-sectional geometry of the blade spar was designed to provide large enough area and area moments of inertia to resist 1.5 times the forces the blades are expected to experience during the mission.

7 Structural Design

7.1 Structural Truss Design

The airframe is designed to be weight efficient while accommodating all eighteen rotors as shown in Figure 7.1. The rotors are placed in a regular hexagonal shape to be compact to minimize structural weight over other arrangements without compromising rotor efficiency. It also provides for a large payload to be located in the center, minimizing aerodynamic downloads.

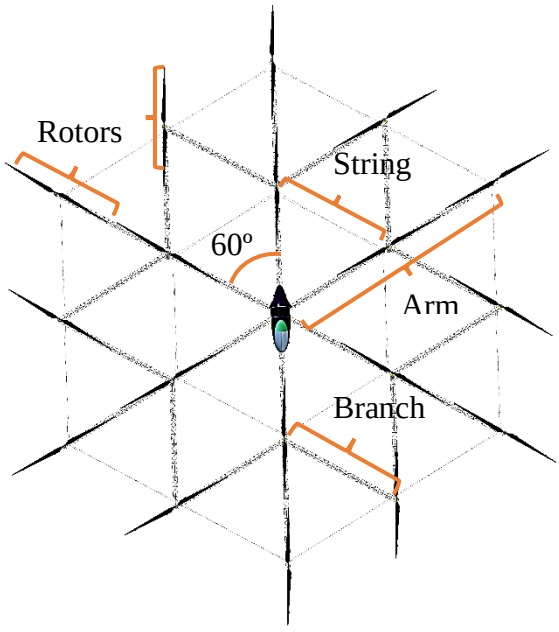

Figure 7.1 Top view of the Chezoía vehicle.

The structure consists of six arms cantilevered from the center of the vehicle. Each of the six arms directly support two rotors, at mid-span and the tip for a total of twelve rotors. The rotor radius is 5.5 ft (1.68 m) so the arms were designed to be 13 ft (3.96 m) long, allowing a clearance of 1 ft around each rotor disk to prevent any blade strikes. There are six rotors not directly supported by the arms. The loads of these rotors are supported by a total of twelve branches. Each arm has a pair of arms branching outwards at 60 degree angles as seen in Figure 7.1. The structure is

designed for a load of 1.5 times the hover thrust to account for control maneuvers and forward flight requirements.

Each arm and branch are designed in a triangular truss pattern as shown in Figure 7.2. The arm design is based on the highly efficient carbon fiber truss structures used on the *Gamera* human powered helicopter [12].

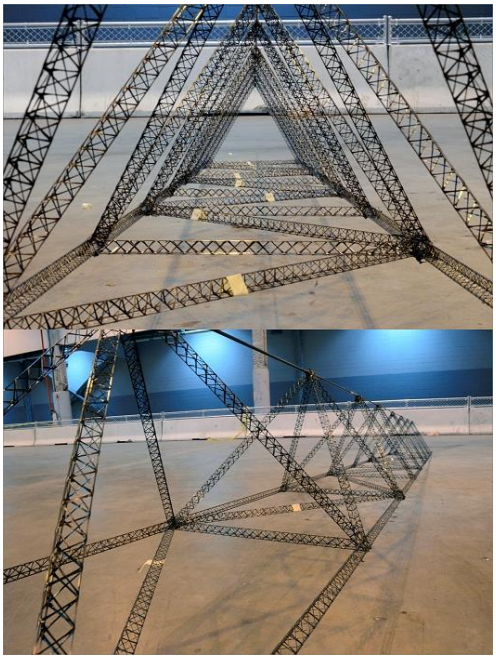

Figure 7.2 Fully constructed Gamera microtruss arm.

The top two members of the truss are designed to sustain compressive forces in flight while the bottom members resist tensile forces in flight. The tensile members are manufactured using commercially available carbon fiber tubes. The compressive members are based on the micro-trusses used on the *Gamera* helicopter [12]. The design philosophy that led to the development of the truss based structures was that the nonlinear impact of thickness on buckling could be used to the designer's advantage if the structural material were concentrated in discrete members instead of being dispersed evenly over the surface of the beam. The microtrusses are composed of three carbon fiber rods connected by a carbon fiber tow shear web as shown in Figure 7.2. The shear web of the beam is constructed from unidirectional graphite-epoxy at ±45° angles, optimal for carrying both shear loads and the torsion loads. Testing of these micro-trusses showed them to be 620% stronger than commercial carbon fiber tubes of the same weight [32]. The structure is designed to be built out-of-autoclave, saving money and eliminating complex manufacturing. The techniques developed for *Gamera* also allows for speedy construction and assembly of the structure [32] The carbon fiber rods of the micro-trusses are limited to a minimum diameter of 1/16 in (1.6 mm) to enable manufacturing by hand. This is very important given the amount of structure required for *Chezoía*'s configuration.

The outer half of the arms, the branches, and the inner half of the arms all experience different loads and so have differently sized members. The inner half of the arms support both the inner set of rotors and the effective moments of the outer ring transferred by both the outer half and branches. The compression members are sized based on the diameter required to resist buckling loads while tensile members are sized in order to not fail under axial stress; hence, twice the number of compression members.

Crossed, high-tensile strength string is strung between rotors tangentially both at the arm tips and at the mid-span as shown in the Structural Overview foldout. The string serves to resist lateral movement and twisting due to rotor torsion. Because of the relatively long arms and relatively low motor torques, more substantial members are not required.

Structural Overview

Innovative microtruss structure

Microtrusses are 620% more efficient than carbon fiber tubes

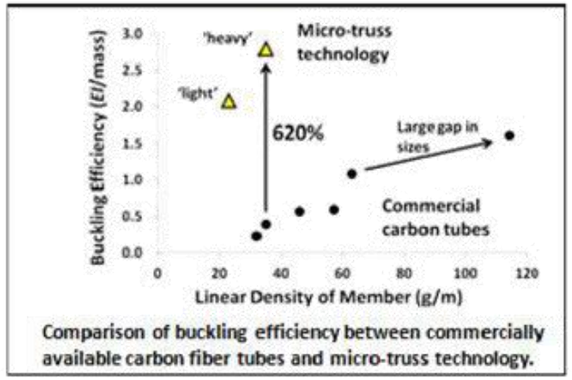

Comparison of buckling efficiency between commercially available carbon fiber tubes and micro-truss technology.

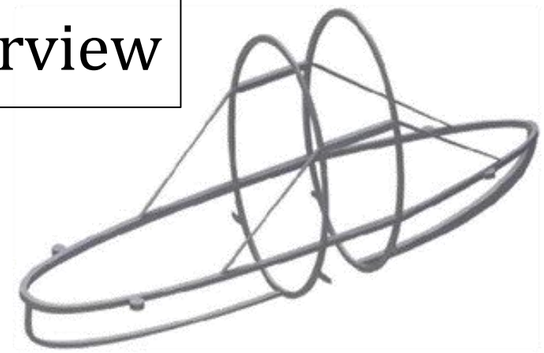

Lightweight fuselage frame

Parameter	Value
Arms	6
Total Arm Weight	86.8 lb
Branches	12
Total Branch Weight	85.7 lb
Stringers	468 ft
Stringer Weight	.516 lb
Total Weight	173 lb

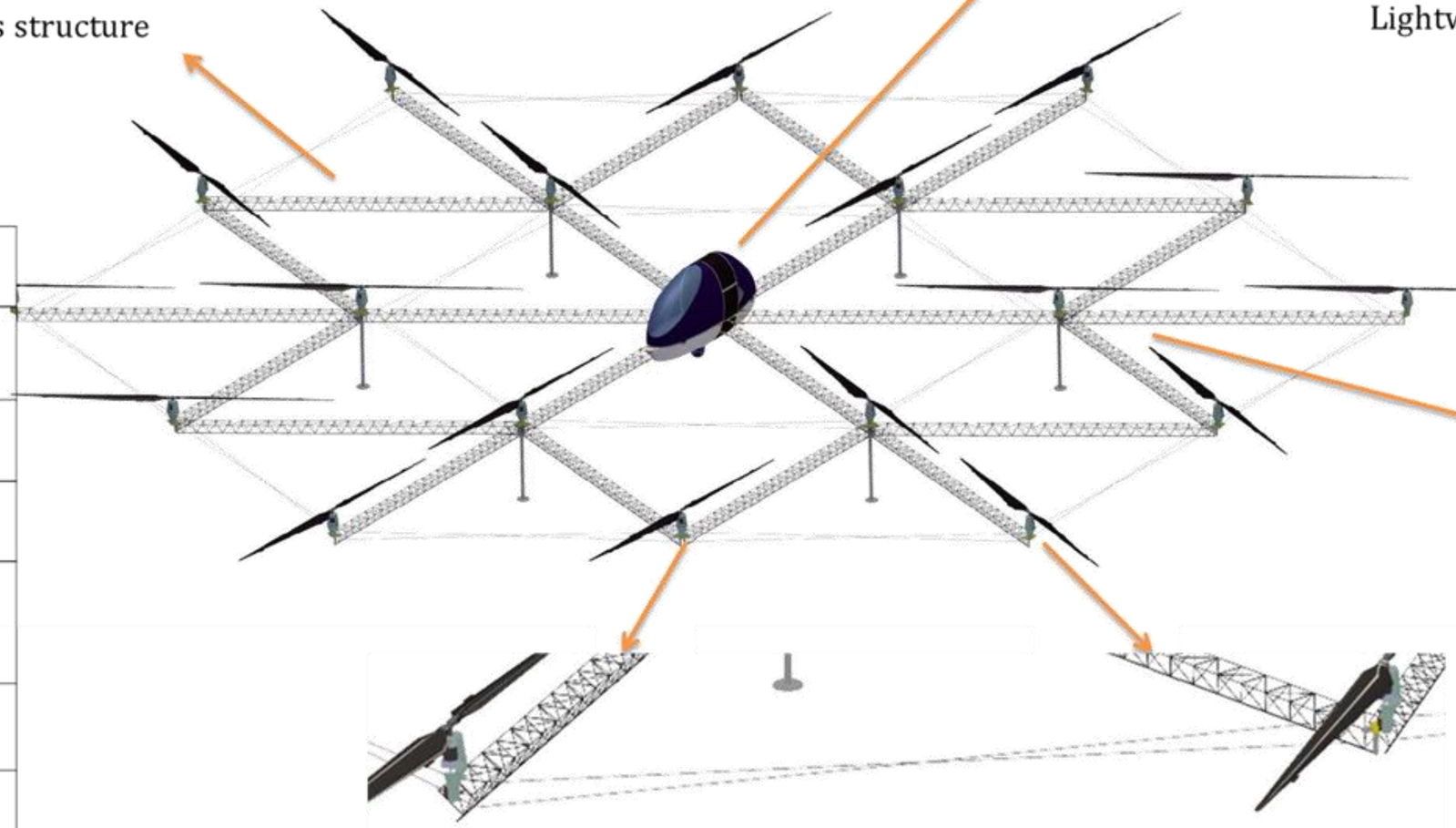

High tensile strength string resists torsional loads

Lightweight landing gear

7.2 Fuselage Design

The fuselage was designed to structurally support the fuel, powertrain, and payload while minimizing weight and aerodynamic drag. High strength-to-weight ratio materials and a streamlined pseudo-elliptical shape are used to achieve these goals. The configuration of various components within the fuselage was chosen to balance the center of gravity of the vehicle about the geometric center.

The core of the structure is a frame made up of hollow aluminum tubes and can be seen in Figure 7.1.a. The aluminum used is anodized Al-7075, which is used for corrosion resistance and high strength-to-weight. The structural members are all hollow, which allows for electrical conduit to connect different parts of the electronics. The frame provides bulkheads for the attachment of the trusses and segments the vehicle into three primary sections: the payload, the fuel tank, and the drive train.

The skin of the vehicle is made up of lightweight Kevlar composite fabric. The front and rear covers do not resist any structural load, and are each attachable at two connection points.

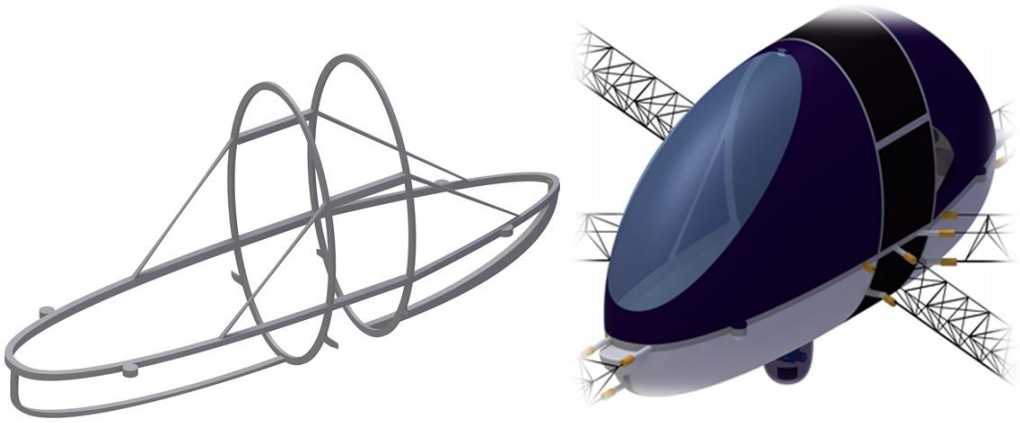

(a) Internal aluminum frame *(b) Assembled fuselage*

Figure 7.1: The center section.

The front section of the fuselage, featured in Figure 7.1.b, is primarily designed to accommodate the payload. The volume of the front section is sufficient for a 95th percentile male to sit [13]. Underneath the "seat" of the payload is the control electronics. The electronics have vents to the outside air to allow for cooling. The seat can also be lifted to allow installation and modification of the electronics. Attached below the electronics stand is a lower fairing housing the side view cameras and LiDAR.

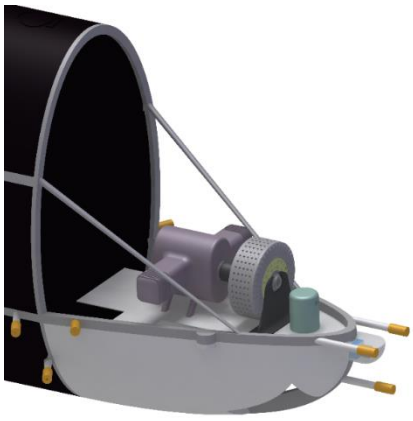

Figure 7.2: Fuselage with the rear cover removed.

The middle section between the two bulkheads is reserved for the fuel tank. The fuel tank center is directly aligned with the geometric center so that as fuel is burned the center

of gravity does not move. The fuel tank is fillable via a hatch in the top of the fuselage. Within each vertical bulkhead is a titanium firewall to protect the front and rear sections.

The rear section contains the drive train and cooling components. An aluminum plate spans the horizontal arch of the rear frame. The generator, engine, and auxiliary components are attached to this plate, and are as far away as possible from the fuel tank section to improve safety and balance the center of gravity of the heavy payload in the front. The engine and generator are connected through tubes to the coolant pump and radiator, which is located at the bottom of the rear. The radiator has a fan which helps push air through the radiator and draw in oxygenated air into the rear compartment for the engine, even when not in forward flight.

In addition, a fore and aft sensor housing are attached to the fuselage. The forward housing contains two thermal cameras and a monocular vision camera to aid forward autonomous flight. The aft section has a single monocular vision camera. The antennae for all external communication from the avionics package have been integrated within the skin of the fuselage.

7.3 Rotor Hub Design

The hub assemblies serve as housing for each rotors drivetrain, connects to the structural truss members, and transfers the thrust from the rotor to the structural members. Each hub consists of a frame connected to a ducted housing structure. In the bottom of the duct is the motor. Connected to the motor shaft is a small fan used to draw air through the motor for cooling. The motor shaft extends to a gear box which is mounted to the top of the duct structure. The gearbox output shaft is coupled with an anodized aluminum connection to the blades and the shaft. This connection supports each blade with two bolts on either side of the center of pressure (¼ chord) of the rotor.

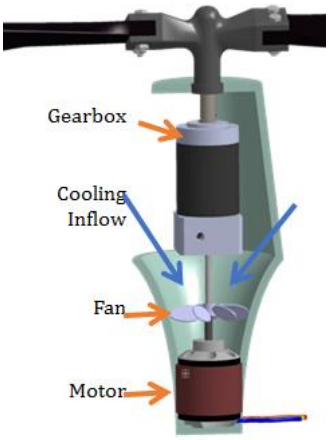

Figure 7.3: Side view cutout of the hub.

Additionally, the hubs are oriented upwards, placing the rotors above the rest of *Chezoía*'s structure. This promotes laminar flow on the rotors when compared to placement of the rotors below the structure. Prioritizing laminar flow allows for the higher power loading by avoiding the profile power increases associated with rotors in turbulent flow. For similar reasons, coaxial rotors were not explored.

8 Vehicle Performance Analysis

8.1 Drag Estimation

Drag reduction was not a primary driver of the design as forward flight and climb time is minimal. The large exposed structure leads to a relatively large equivalent flat plate area. The drag of each component was estimated using results from *Fluid Dynamic Drag* [14]. The resulting flat plate areas of the various components are shown in Table 8.1. The total horizontal flat plate drag area is 39.8 ft^2. The horizontal flat plate sideforce area is somewhat larger at 56.4 ft^2. The vehicle is highly symmetric and the fuselage is mostly uncambered so the equivalent flat

plate lift area is assumed to be negligible. The drag force on the fuselage acts slightly above the geometric center and so the equivalent pitching moment area is 2.81 ft^3.

Table 8.1: Equivalent flat plate area estimates for Chezoía's various components.

Component	C_{Dx}	C_{Dy}	C_{Dz}	Flat Plate Drag Area (ft^2)	Percent of Total Drag Area
Fuselage	0.20	1.0	0.25	4.23 (0.39 m^2)	10.7%
Rotor Hubs	1.1	1.1	0.2	9.9 (0.92 m^2)	25.0%
Landing Gear	1.1	1.1	1.7	4.12 (0.38 m^2)	10.4%
Trusses	1.1	1.1	1.1	21.5 (2.00 m^2)	54.0%

8.2 Forward Flight Performance

The focus on hover and limiting structural weight results in *Chezoía* having a relatively high drag due to structure design and small excess installed power. Because of these characteristics, *Chezoía* is ideal for endurance missions, but has lower maximum speeds than typical helicopters. The maximum level flight speed is 37.6 knots (19.3 m/s) corresponding to an advance ratio of 0.24, which is still fast enough to traverse the 0.54 nm (1 km) between hover stations in under 30 seconds. The calculated induced, profile, and parasitic power curves can be seen in the Rotor and Vehicle Performance foldout. From these curves, the velocity for minimum power (V_{BE}) was calculated to be 18.3 knots (9.41 m/s), and the velocity for maximum range (V_{BR}) was calculated to be 24.1 knots (12.4 m/s).

However, as a hovering endurance helicopter, *Chezoía* has strong performance in maximum range and maximum time aloft. These characteristics make it ideal for mission choices where long distances or long air time missions are necessary such as surveillance or payload delivery. The range and endurance parameters of the vehicle are summarized in Table 8.2. These performance parameters are much greater than typical light helicopters like the R22, which has a maximum range of 250 nm (463 km) and a flight time of less than 4 hours.

Table 8.2: Endurance parameters starting from a takeoff weight of 1010 lb.

Maximum Hover Time	25 hours
Maximum Range	717 nautical miles (1329 km)
Maximum Endurance Time (at V_{BE})	32.6 hours

8.3 Axial Climb and Descent

The climb rate was determined in hover and in forward flight. In hover at takeoff weight, the vehicle can climb at a rate of 5.8 ft/s (1.77 m/s), meaning the vehicle can reach an altitude of 2 vehicle diameters,126 ft (38.4 m), in under 30 seconds. The maximum rate of climb in forward flight is 14.2 ft/s (4.33 m/s) at a forward speed of 18.3 knots (9.41 m/s).

The induced velocity in hover was determined to be 11.1 ft/s (3.38 m/s) from basic momentum theory. This value is relatively low as a result of the low disk loading of the vehicle. Therefore, it is recommended that the vehicle descends at a rate greater than 22.2 ft/s (6.77 m/s) to avoid vortex ring state if at high altitudes. However, for the required mission the operating altitude will

only be a couple hundred feet and a descent rate of less than 5.5 ft/s (1.68 m/s) should be used to avoid power settling.

The hover ceiling was determined to be 7,040 ft (2146 m) using standard atmospheric tables due to a decrease in power available at higher altitudes. This value is somewhat comparable to lower than the R22's OGE hover ceiling at 1,300 lb (590 kg) of approximately 8,000 ft (2438 m).

9 Power System Overview

Energy is converted through a number of steps from combustion to thrust production. For *Chezoía's* energy production and conversion, a diesel engine is connected to an electric generator through a direct drive. The generator produces high voltage electrical power. A small portion (less than 0.2 hp) of this electrical power is directed to the electronics required for autonomy. The rest of the power is sent to the electric motors where it is rectified and stepped to the appropriate voltage at the hubs to reduce wire weight. The auxiliary battery in the electronics can also transmit power to the rotors for an emergency descent in the event of a power failure. Finally, the electric motors transmit electrical power through the gearboxes to the thrust-producing rotors. A schematic representation of this process can be seen in Figure 9.1.

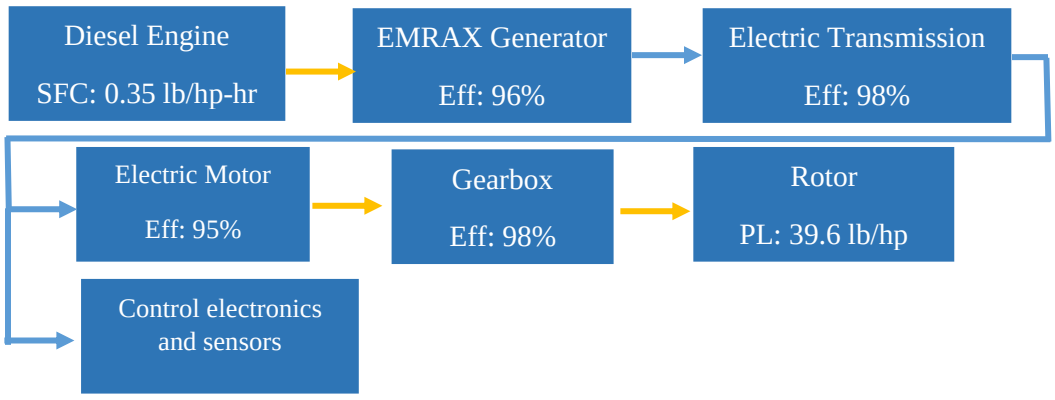

Figure 9.1: Energy transmission and typical values during hover. Yellow arrows indicate mechanical power transmission, and blue arrows indicate electrical energy transmission.

9.1 Powerplant Selection

The powerplant consists of two components, a diesel engine and a generator. The diesel and generator are located within the aft section of the fuselage. The two components of the powerplant are connected directly by a shaft with flexible couplings to allow for small misalignments.

Rotor and Vehicle Performance

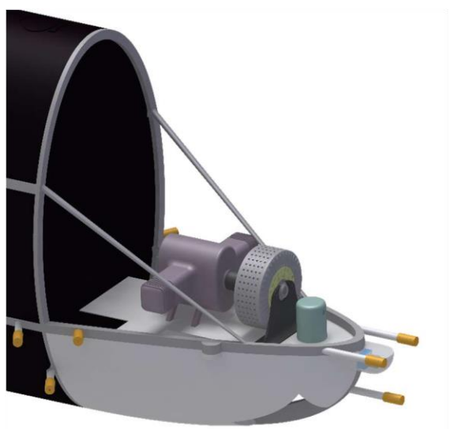

Rotor Parameters

Rotor Parameter	Value
C_T	0.0037
C_P	$1.96 \cdot 10^{-4}$
FM	0.803
K (induced power factor)	1.0475
Taper Ratio	0.144
Twist (Root to Tip)	6.39º
AR	20.5
C_T/σ	0.175

Tip Speed Control

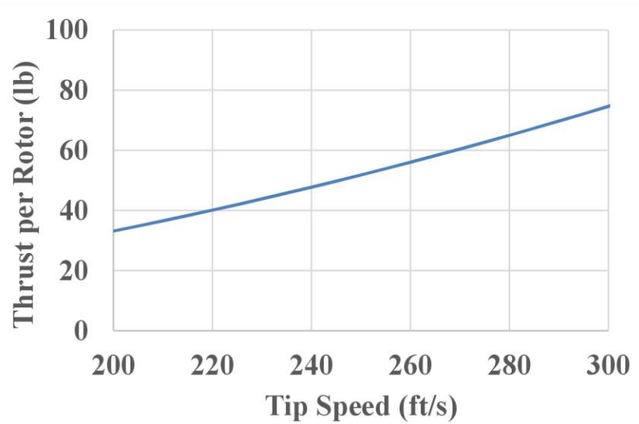

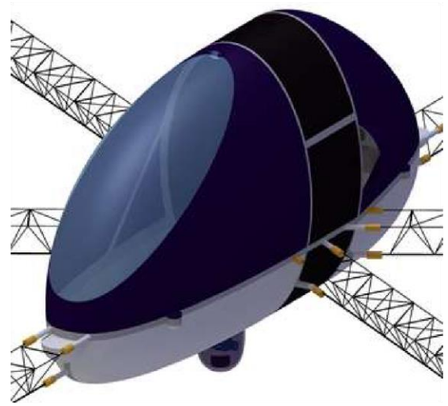

Forward Flight

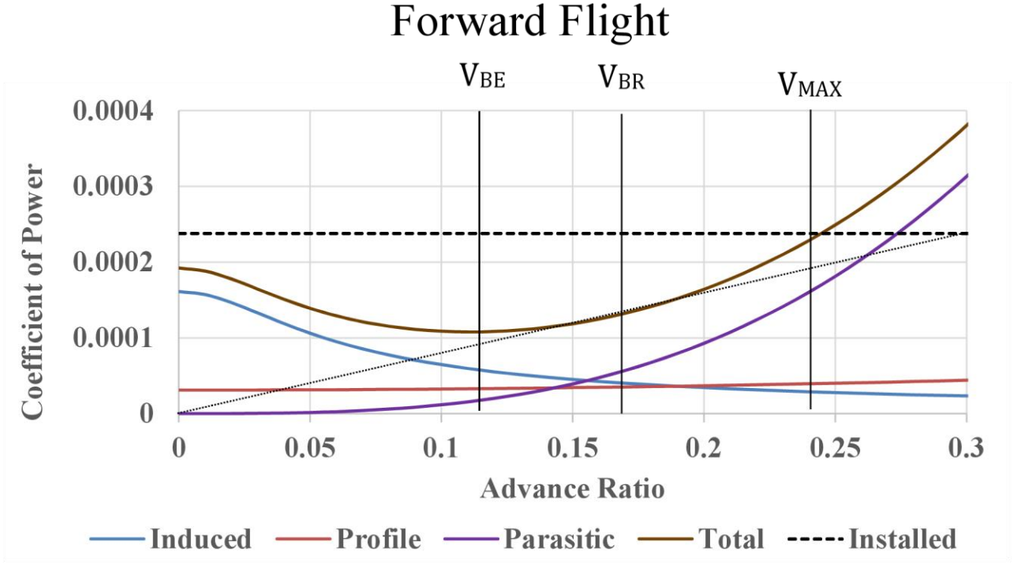

Vehicle Range and Endurance

Maximum Hover Time	25 hours
Maximum Range	717 nautical miles
Maximum Endurance Time (at V_{BE})	32.6 hours

9.1.1 *Engine Selection*

A "rubber" engine has been selected for *Chezoía*. An analysis of existing diesel engines was the starting point for selecting the design parameters for the rubber engine. The power-to-weight ratios for a variety of commercially available diesel engines are shown in Figure 9.3. It is apparent that a feasible rubber engine could have a power-to-weight ratio of 0.5 lb/hp (0.30 kg/kW), and a specific fuel consumption (SFC) of 0.35 lb/hp-hr (0.21 kg/kW-hr). A 35 hp (26.1 kW) engine was chosen to provide sufficient power to *Chezoía* which corresponds with an engine that is 70 lb (31.8 kg). The rubber engine also operates at up to 4000 RPM, comparable to the current engines investigated.

While the engines presented in Figure 9.3 are within the 135 – 200 hp (100 – 150 kW) range, the SFC and power-to-weight ratios do not vary widely within this range. Commercially available diesel engines at lower power ratings, such as the Audi TDI 100 [15], have an even greater fuel efficiency with an SFC of 0.326 lb/hp-hr (0.198 kg/kW-hr). For these reasons, it was determined that it is technically feasible within 5 years to develop a diesel engine at *Chezoía's* required engine power.

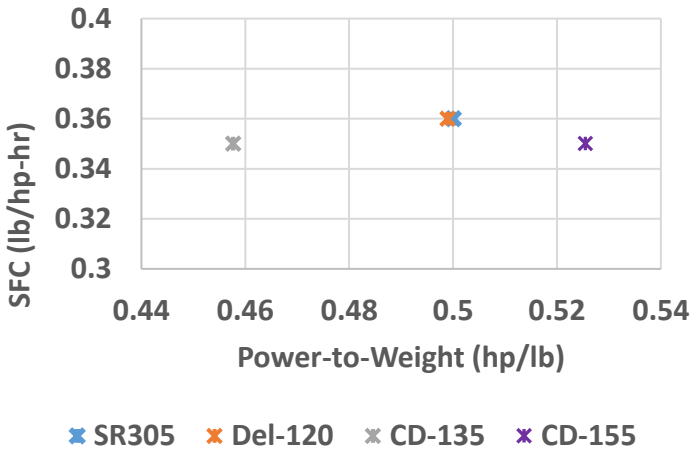

Figure 9.3: Performance characteristics of existing diesel engines.

A flat diesel has been selected for *Chezoía*. This selection was made because the configuration reduces vibrations and each cylinder has maximal surface area for cooling. Only two cylinders are required for the engine as well, because of the low power requirements. In addition, because the selected engine is a diesel engine, the SFC is approximately constant through the range of idle power through maximum rated power.

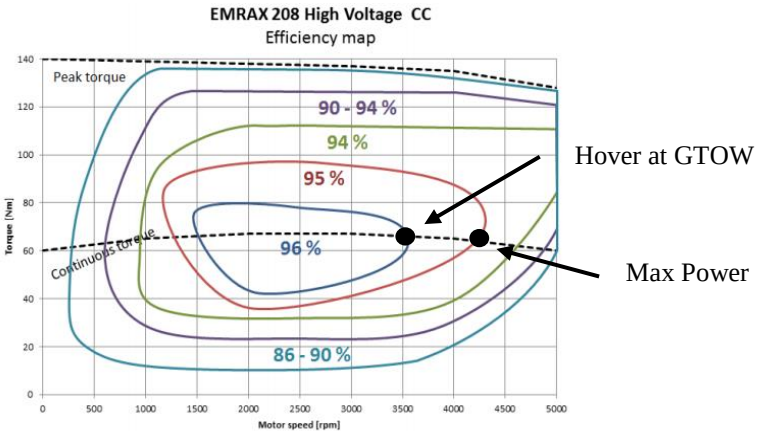

Figure 9.2: Efficiency map of the EMRAX 208 brushless AC motor. [33]

9.1.2 *Generator Selection*

The selected generator for *Chezoía* is the Emrax 208, a brushless AC motor. The low voltage, liquid cooled variant will be used, to reduce the potential for arcing and to improve the heat dissipation of the generator. The generator can provide up to 43 hp (32 kW) of continuous power

and is fairly lightweight at 20.3 lb (9.21 kg). An efficiency map can be seen in Figure 9.2. From this figure, it can be seen that throughout its operating regime the generator is 95-96% efficient, with hover at GTOW occurring at 3500 in the 96% efficiency region.

9.2 Electric Transmission

Power from the generator will be transferred to each of the rotors through individual motor and gearbox combinations. The decision to utilize an electric transmission was made based on multiple advantages which it provided over a direct mechanical drive. The electric transmission facilitates the use of RPM control for the rotors, and allows for a substantially simpler hub design, without the need for either collective or cyclic controls. This simplicity greatly reduces the weight of the hub for each rotor as well as the reliability of each assembly, which is an important advantage because the vehicle has 18 rotors. In addition, the electric transmission avoids the weight of heavy drive shafts spanning the length of the structure, in favor of lighter wiring to transfer power. The electric transmission consists of three components for each rotor: a motor, gearbox, and electronic speed controller.

9.2.1 Motor Selection

To select *Chezoía's* motors, a study was performed to examine state of the art commercially available motors. Data was compiled on a variety of motors before focusing on brushless DC motors, for their power to weight and efficiency advantages. To maximize efficiency, *Chezoía* utilizes "rubber" motors which are specialized for the power and RPM requirements of its mission. The process of designing these motors consisted of analyzing the data from existing motors and fitting trends to determine characteristics and expected performance of motors which would be developed within the next five years.

This can be seen in Figure 9.4 which shows the process as completed for determining the weight, RPM constant, and price of the motor, directly from the power requirements of *Chezoía's* mission. The figure shows the weights of 13 currently available electric DC motors in the 0.5-4.5 hp (0.4-3.5 kW) range. The trend line shows the range of weights for the lighter available motors, this trend was used to extrapolate the weight of a motor with the calculated power requirement of 1.61 hp (1.2 kW).

A similar procedure was followed in order to determine realistic parameters for the other parts of the motor such as the RPM constant (Kv), torque, and price. The results of the motor selection process showed that motors with the required power output of 1.61 hp (1.2 kW) have a weight of 0.65 lbs (294.5 g), a torque at the output shaft of 0.74 ft-lbs (1.59 Nm), and an efficiency at the operating RPM of 95%.

9.2.2 Gearbox Selection

In a similar way, the gearboxes used with *Chezoía's* rotors are also designed specifically to the requirements of its mission. A survey of current commercial gearboxes was completed and a database compiled. The selection was narrowed by focusing on planetary gearboxes, specifically for their reliability, ease of integration, and efficiency in *Chezoía's* system.

Starting from the design points of *Chezoía's* selected motors, the parameters utilized for selection were the input torque and RPM from the motors and the required RPM for *Chezoía's* rotors. Trends from commercially available gearboxes were analyzed and extrapolated to determine characteristics for the custom designed gearboxes. Figure 9.5 shows the weight, input RPM and price as a function of the maximum torque for the selected gearboxes. For *Chezoía*, this results in each gearbox having a weight of 1.38 lb, a maximum RPM of 14800, and price of $380.

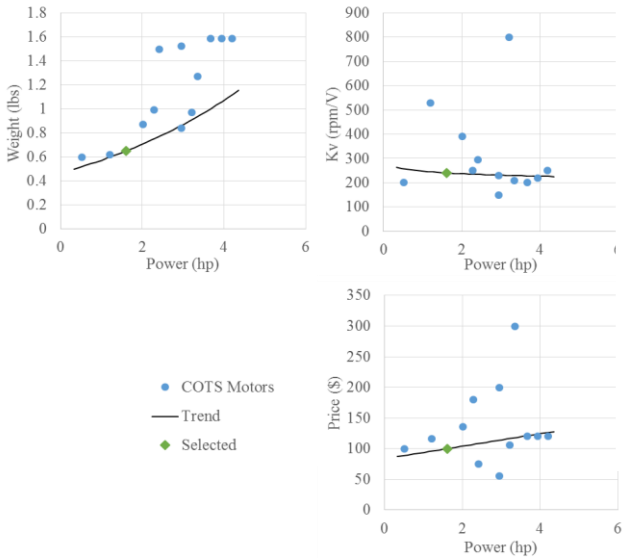

Figure 9.4: Weight, Kv, and price for BLDC motors as a function of power

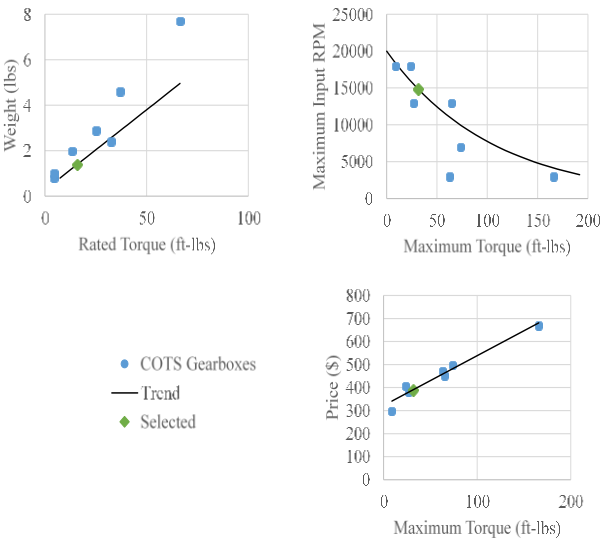

Figure 9.5: Weight, RPM, and price trends for gearboxes as a function of maximum torque

9.2.3 Electronic Speed Control

Electronic speed controllers (ESC) are used to control the RPM and torque of each of *Chezoía's* 18 rotors. The Turnigy Super Brain 100A Brushless ESC was selected for this due to its compatibility with the target voltages and currents that are needed through the motors [16]. Each controller will receive signals from *Chezoía's* autopilot in order to implement RPM controls with the rotor system.

9.3 Cooling System

Cooling is an important and critical system to ensure that the engine, generator, and motors function continuously for 24 hours without overheating. The diesel engine and the generator require liquid cooling. The weight of the radiator, fan, coolant and coolant pump of *Chezoía* is estimated as 15 lb (6.80 kg). The radiator includes a fan to draw a sufficient mass flow of air and can be seen in Figure 9.6. The hot air from the radiator is exhausted out through an outlet in the bottom of the fuselage as

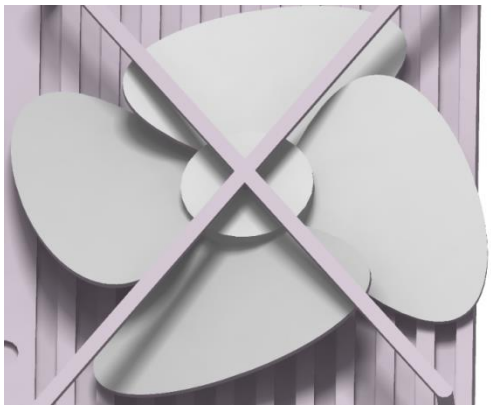

Figure 9.6: Close up view of fan over the radiator.

seen in Figure 9.7. The pump draws a water and ethylene glycol mix through hoses connected to the engine and generator.

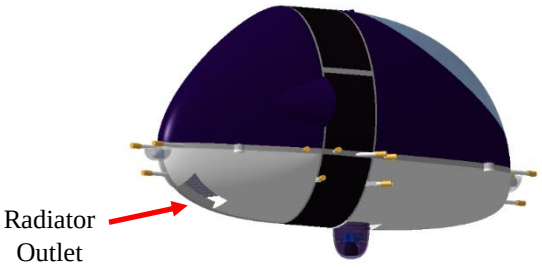

Figure 9.7: Rear view of the fuselage with the radiator outlet highlighted.

The electric motors rely on air cooling, since it would be impractical and unnecessary to have water cooling for the high efficiency electric motors. A small ducted fan connected to the shaft of the motor before the gearbox induces airflow through the coils of the electric motor. Due to the multirotor design, this system offers enough cooling for each of the motors. Based on the power and efficiency of the motors, ambient temperature of 90°F (32°C), and an allowable motor temperature of 120°F (49°C) [17], the airflow necessary for cooling each motor is 8.93 ft^3/min (4.2×10^6 mm^3/s). These calculations agree well with a CFD based study completed at the University of Bielsko-Biala [18], which found that for a motor with 25% higher heat energy to be dissipated, the necessary airflow was 11.65 ft^3/min (5.5×10^6 mm^3/s), 30% higher than the calculated requirement for *Chezoía's* motors.

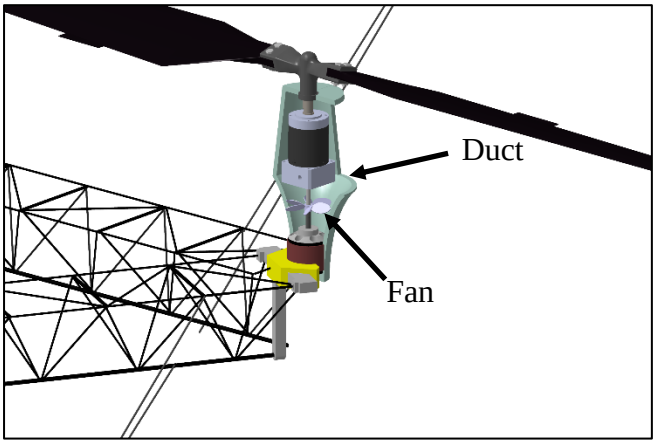

Figure 9.8: Cutaway view of the rotor hub assembly showing the innovative cooling fan.

To achieve this cooling for each motor, the hub was designed to allow airflow as well as include a cooling fan on the drive shaft, as can be seen in Figure 9.8.

9.4 Lubrication System

The lubrication system serves two purposes: reduce friction of the diesel engine, and remove some heat. The engine has a built in oil pump and filter which circulates lubricant throughout the combustion engine.

9.5 Emergency Battery

Chezoía has been equipped with a 1.6 hp·h (1.2 kWh) emergency battery. With a power density of 0.078 hp·h/lb (128 Wh/kg), this battery weighs 21 lbs (9.5 kg) and provides *Chezoía* with 3.3 minutes of flight time in the case of main powerplant failure.

10 Avionics and Sensors

Chezoía's Avionics and Sensors package has been designed to facilitate full autonomy throughout its mission. Through full autonomy, the vehicle can ensure better reliability through the elimination of pilot error and fatigue over the course of a more than 24 hour mission. The

package utilizes a variety of commercially available technologies and products in order to ensure dependability and redundancy while also minimizing weight, price, and power consumption.

10.1 Mission Requirements

The complete mission of *Chezoía* comprises vehicle takeoff, extended periods of hover, with short intervals of forward flight, before landing back at the original takeoff point. From the RFP, the avionics package must allow for the aircraft to be unoccupied, hover within three separate hover stations, and allow for disturbance rejection for winds up to 9.71 knots (5 m/s). Additionally, the RFP requires a basic mission profile as discussed in Section 2.1. With this profile, the mission is broken into several segments which fall under one of the following categories.

- **Take-off:** During this phase, the vehicle must maintain control while gaining altitude to a point no less than twice its largest dimension off the ground. For *Chezoía*, this will entail rising to an altitude of roughly 150 feet (45 m).
- **Forward Flight:** To fly between hover stations, *Chezoía* will have to go through forward flight of at least 0.54 nm (1 km). During this time, the vehicle should be able to maintain control as well as detect and properly avoid obstacles which may exist in its path.
- **Hover:** The major part of the mission will be spent in this phase. In each phase of hover, the vehicle must be able to maintain zero relative velocity with respect to a ground observer station as well as maintain a constant altitude. Additionally, the vehicle must maintain a position within the pre-prescribed sphere with radius 65 feet (20 m).
- **Landing:** For successful landing, the vehicle must be able to safely descend from its hovering altitude to the ground and then shutdown to complete the mission.

Throughout all phases of the mission, the avionics suite should also maintain redundancy and systems monitoring such that malfunctions can be detected and either adjusted for to continue the mission or to ensure the safe descent of the vehicle returning to the ground.

Figure 10.1: Individual units of both the basic and advanced avionics packages.

10.2 Sensors and Selected Equipment

When developing the avionics suite for use on *Chezoía*, a broad study of available technologies was conducted in order to ensure the most effective and efficient package possible. The available technologies were evaluated based on the RFP requirements which they would contribute towards, as well as their weight and power consumption. A basic package was assembled, as well as additional sensors for increased mission capabilities. The units included in both these packages can be seen below in Figure 10.1. From left to right, the units are the VECTOR, TELEM05, mvBlueFOX3, LPC-480G4, Quark 640, Sweep V1, and XPS-TR. Antennae for all communications have been integrated within the skin of the fuselage section.

10.2.1 Basic Avionics Package

- **UAV Navigation VECTOR Autopilot:** *Chezoía* utilizes the VECTOR as its primary navigational unit for facilitating flight and position tracking throughout the completion of its mission. The autopilot is capable of controlling *Chezoía* through all phases of its mission from startup to shutdown using integrated GPS and INS systems. It provides position accurate to within 6.56 ft (2.0 m) as well as pitch and roll within 0.5° and heading within 1°. In addition, the unit has 62 I/O lines to support flight control information for each of *Chezoía's* 18 rotors individually. Redundant sensors, power supplies, and internal monitoring make it reliable even after individual sensors may experience failure [19].
- **UAV Navigation TELEM05:** VECTOR will be able to send and receive signals through TELEM05. This unit has a range of 52 nm (100 km) to facilitate remote missions while still maintaining proper communication with the unmanned vehicle. As part of the package, it is also lightweight and low power, making it the choice for *Chezoía's* suite [20].
- **TE Connectivity Ni1000SOT:** Over the course of achieving 24 hour hover, *Chezoía's* motors will experience heating from use. Each motor will be equipped with an Ni1000SOT temperature sensor to monitor the temperature of all 18 motors, allowing the flight controller to determine a drop rotation for cooling purposes. These sensors are effective from -67°F to 320°F (-55°C to 160°C) allowing for readings within 1°C through the full range of temperatures the motors may experience [21].
- **Eaton DCCS50-100:** Similarly, each of the 18 motors will also be equipped with a DCCS50-100 current sensor to monitor the performance of each motor, gearbox, and rotor assembly [22]. With this information, the flight controller will be able to identify damaged or inoperative assemblies based on current spikes or drops. Once identified, the flight controller can remove such rotors from the rotation and mission operation can continue with the other rotors making up the difference.
- **Fenix E35UE:** FAA rules require proper position and anti-collision lighting for aircraft. The Fenix E35UE LED lights will serve to satisfy these requirements and ensure visibility for *Chezoía* during flight time [23]. As required, there will be a red LED on the outside of the starboard side rotor hub, a green LED on the outside of the port side rotor hub, and white LEDs on the fore and aft rotor hubs.

10.2.2 Advanced Optional Avionics

While the basic sensor package listed above allows *Chezoía* to complete its prescribed mission, the sensors and equipment listed below augment that package to extend its mission capabilities to more locations, especially through advanced autonomous obstacle avoidance techniques. The fields of view provided by these sensors can be seen in Figure 10.2. The four BlueFox3 cameras provide a 360° view (blue shading), two Quark thermal cameras provide a 120° forward view (orange shading), and the Sweep V1 provides a 360° view with range of 500 feet (150 m) (grey shading).

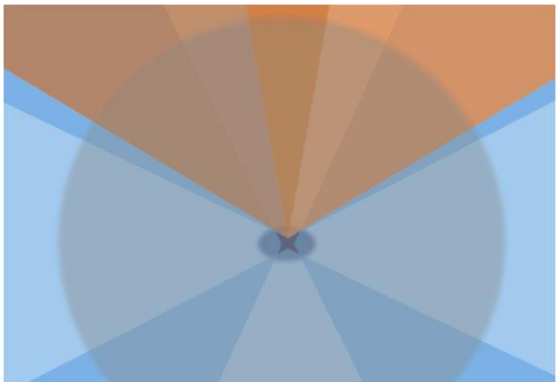

Figure 10.2: Advanced obstacle avoidance fields of view.

- **mvBlueFOX3:** The BlueFOX3 paired with an MV-O-SMOUNT 03.2 IRC E10M3220 lens provides a camera solution capable of supplying images for use in Large-Scale Direct Monocular Simultaneous Localization and Mapping (LSD-SLAM). This pair provides an image with a 129° viewing angle, captured using a global shutter which is necessary for creating accurate depth maps due to the motion blur of a rolling shutter [24]. Four cameras will provide 360° vision around the vehicle with 88° of vertical vision as well, meaning that with this addition to the sensor suite, *Chezoía* could be piloted remotely as well [25].
- **Sparton LPC-480G4:** Used to run the LSD-SLAM algorithms and determine locations of obstacles. The unit runs with an Intel 3rd Generation Core i7 Processor 3610QE, 16GB of RAM, and 1TB of storage capacity, which provides sufficient computational power to run algorithms for each of the four cameras as well as integrating the depth maps together [26] [27]. It includes an internal cooling fan and temperature monitoring as well, to facilitate cooling and early warning in the case of overheating.
- **Quark 640:** Two Quark 640 thermal imaging cameras will be able to provide improved awareness of live or moving obstacles such as birds or other aircraft based on their heat signature. Each camera provides a 69° viewing angle, allowing for thermal imaging support for the 120° in front of the aircraft [28]. This data can then be integrated with the LSD-SLAM results to improve object detection.
- **Sweep V1 360°:** The Sweep is a rotating LiDAR distance sensor for additional redundancy and improved object detection in low-light conditions that may arise within the span of a 24 hour mission. Due to its reliance on lasers, it can augment the existing LSD-SLAM system during low-light conditions when the BlueFOX is less effective. However, its range is limited to about 500 ft. (150 m), limiting its effectiveness as a standalone obstacle detection system [29].
- **XPS-TR:** New FAA rules require that by 2020, all aircraft flying within a variety of airspaces will have Automatic Dependent Surveillance-Broadcast (ADS-B) equipment.

The XPS-TR transponder will satisfy this requirement and allow *Chezoía* to be flown under FAA rules, opening more mission profiles for completion [30].

10.3 Sensor Operation During Flight

During flight, *Chezoía's* base avionics package is mainly centered around the operation of its VECTOR autopilot. Throughout all phases of the mission, the autopilot will determine the attitude of the aircraft based on internal Kalman filter estimation with the VECTOR's gyroscope and accelerometer measurements. It will also track and transmit the aircraft's altitude and geographic location though the TELEM05 unit connected to the autopilot.

10.3.1 Obstacle Identification

When utilizing the base avionics package, *Chezoía's* flight path will be preloaded into the autopilot, avoiding obstacles such as buildings and large trees. This package is suitable for experimental flights or flights in clear locations with well-known topography and geography, however, for more dynamic and adaptive flight plan capabilities, *Chezoía's* optional avionics package is necessary. Advanced obstacle avoidance during forward flight will be completed using the optional cameras and CPU described above in Section 10.2.

From the images provided by the four BlueFox cameras, the Sparton CPU will use the LSD-SLAM method of Engel, Schöps, and Cremers in order to develop a three dimensional depth map of the aircraft's environment [31]. From this depth map, the CPU will detect obstacles based on the depths which are returned. Similarly, data from the thermal imaging cameras and LiDAR sweep will supplement this as additional sources of obstacle detection fed to the Sparton CPU. The CPU will then integrate this data to output any perceived obstacles to the autopilot to be avoided with a turning maneuver as well as updating the original planned path with waypoints around the obstacle, based on the depth readings taken.

10.3.2 Motor and Rotor Diagnostics

The inclusion of the Ni1000SOT and DCCS50-100 with each hub assembly allows for tracking of motor diagnostics in real time during flight. Each temperature and current sensor takes data corresponding to one of the 18 rotors, and relays this data to the CPU. With temperature readings, the CPU can detect if a motor is running too hot and needs to be shut down to avoid permanent damage. Similarly, the current sensor provides diagnostic information about the performance of the motor and rotor. If the sensor detects a sudden current drop or spike, this could indicate either a failure in the rotor or a seizing of the gearbox respectively. With this information on the health of each rotor assembly, the CPU is able to communicate with the autopilot to shut down individual rotors. Throughout the mission, redundancy in the power plant and control scheme allow for the mission to continue with 2 rotors out at the start and up to 5 rotors out by the end of the mission.

10.4 Avionics Package Power Requirement and Weight Breakdown

Table 10.1, provides a breakdown of *Chezoía's* power requirements, weights, and prices of each component. The total power required for the package is less than 0.2 hp (0.15 kW); the avionics consume less than 1% of the aircraft's total power during hover. Before startup, an auxiliary

battery is included to facilitate diagnostic checking of the avionics, as well as remote startup before the system is powered by the engine.

Table 10.1: Complete list of Avionics and sensors with weight, power, and price breakdown.

Component	Model	#	Power (hp)	Total Power	Weight (lbs)	Total Weight	Price	Total Price
Autopilot	VECTOR	1	0.0034	0.0034	0.397	0.397	$7,500	$7,500
Tranciever	TELEM05	1	0.0087	0.0087	0.397	0.397	$2,000	$2,000
Lights	Fenix E35UE	4	0.0054	0.0215	0.031	0.125	$15	$60
Temperature Monitor	Ni1000SOT	18	0.0000	0.0000	0.022	0.397	$9	$162
Current Sensor	DCCS50-100	18	0.0000	0.0000	0.022	0.397	$8	$144
Visual Cameras	mvBlueFOX3	4	0.0027	0.0107	0.037	0.150	$50	$200
Vision CPU	LPC-480G4	1	0.1126	0.1126	3.439	3.439	$1,440	$1,440
Thermal Cameras	Quark 640	2	0.0017	0.0035	0.060	0.120	$1,500	$3,000
LiDAR	Sweep V1 360°	1	0.0034	0.0034	0.265	0.265	$350	$350
Transponder	XPS-TR	1	0.0107	0.0107	0.220	0.220	$5,200	$5,200
Startup Battery	Dell 451-10339	1	-	-	1.060	1.060	$19	$19
Total				0.1745		6.967		$20,075

Over half of the package's total power and nearly half of its weight is comprised of the LPC-480G4 CPU used for the computations necessary for the optional advanced obstacle avoidance package, meaning that the base configuration weighs less than 4 pounds and uses less than half the power. However, the bulk of the price of the avionics lies with the VECTOR autopilot, as well as the transponder and thermal cameras. Again, the base avionics package costs about half as much as the full package, with prices of $9,885 and $20,075 respectively.

11 Flight Dynamics and Control

The control of the aircraft in hover was a specific requirement for the mission. *Chezoía* has been designed with this in mind, including the requirements on its control scheme. Its 18-rotor design allows for simple RPM control to maintain precision hover capabilities, as well as 3 independent complete sets of control rotors, allowing *Chezoía* to remain fully controllable even in the case of malfunctions with one or more rotors.

11.1 Flight Dynamics Model

Chezoía's flight dynamics model is based largely on existing models of quadcopter designs, extended to reflect its 18-rotor configuration. Aerodynamically, the aircraft consists of the following major components: the 18 rotors and hubs in their hexagonal arrangement, the structural microtrusses which connect the hubs, and the fuselage, including the payload, fuel, engine and generator. These components are the main source of aerodynamic and inertial forces and moments throughout the completion of *Chezoía's* mission.

11.2 Control Scheme

Chezoía is controlled through an innovative control scheme which maps a typical quadcopter control scheme to function as part of its 18-rotor design. This use of a quadcopter control scheme allows for simplicity and reliability within the controls themselves, as well as allowing for redundancies with three separate sets of control rotors which can handle complete pitch and roll control, even with other rotors out or otherwise malfunctioning. In the case of any given rotor system malfunction or dropping a motor for cooling, the VECTOR will distribute the thrust of that rotor between the other 8 rotors rotating with the same directionality to maintain yaw stability.

All rotor controls originate from the autopilot located in the center section of the aircraft. The autopilot works in tandem with each of the 18 electronic speed controllers to maintain and adjust the power to each of the motors, achieving full control of the aircraft.

11.2.1 Differential RPM

Chezoía achieves control entirely through the regulation of power to each of its motors. Due to its multirotor design, the aircraft does not require change in pitch or cyclic controls. Rather all thrust and torque adjustments for the rotors are completed through RPM control. Each rotor's rotational speed is managed by its own electronic speed controller, all of which are connected through the central autopilot.

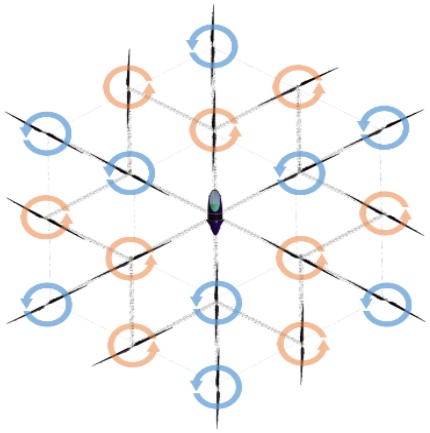

Figure 11.1: Rotor Directions.

11.2.2 Rotor Mapping

The 18-rotor design was created with symmetry, structural integrity, and controllability as design drivers. This results in *Chezoía's* rotor layout consisting of concentric hexagons, with an outer set of 12 rotors and an inner set with 6 rotors. The rotational direction of each rotor is designed with redundancy in mind, alternating the direction of neighboring rotors. This facilitates ease of correction in the case of failure of one or more rotors. The rotational directions of *Chezoía's* rotors are shown in Figure 11.1.

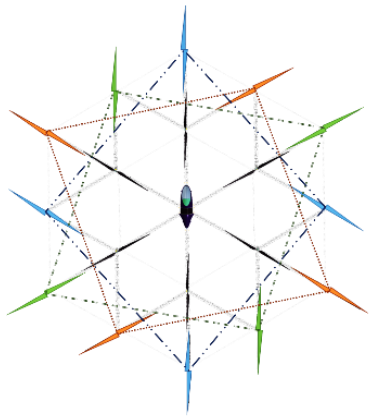

Figure 11.2: Quadcopter control sets.

11.2.3 Roll and Pitch Control

Chezoía implements innovative use of interchangeable quadrotor control sets in order to maintain rolling and pitching control while preserving the ability to elect to shut down rotors during flight for cooling, efficiency, or malfunction reasons. The quadrotor control sets, color coded and shown in Figure 11.2 as being connected by dashed lines, are implemented using only the outer hexagon of 12 rotors, leaving the inner rotors operating at optimal RPM throughout the mission. The outer rotors are grouped into sets of four rotors which comprise three separate quadrotor sets. Each set ensures that adjacent

rotors rotate opposite directions relative to each other, ensuring a control scheme which minimizes coupling connecting roll and pitch controls with yaw controls. Each set is indicated in the figure by its own unique color, either orange, blue, or yellow, with the inner hexagon not used for rolling or pitching controls.

At any given time during a mission, only one of these control sets is in active use, while the others simply maintain nominal thrust to facilitate hovering power. For the control set in use, tested and proven quadcopter algorithms are utilized for rolling and pitching controls with only minor adjustments allowing for the difference in moment arms between the pair of rotors closer and the pair further from the center of each set. With this control set and a maximum trim of 10%, *Chezoía* can achieve maximum control moments of 122.4 ft-lbs (165.9 Nm) in any direction of the rolling and pitching axis.

11.2.4 Yaw Control

While rolling and pitching are controlled exclusively through the quadcopter control sets, *Chezoía* achieves yaw control utilizing all 18 of its rotors. This draws on the additional rotors for more rapid adjustments in attitude. Much like in a quadcopter scheme, rotation about the central axis is completed by slightly raising the RPM of all motors in one direction while lowering motors in the other direction equally, thus creating a rotational moment while maintaining constant thrust to keep the aircraft stationary in altitude. With this scheme, the aircraft can generate yaw moments up to 28.2 ft-lbs (38.2 Nm) around its central axis, using a maximum motor trim of 10% from the nominal power of 1.41 hp (1.05 kW).

11.3 Stability

In order to successfully complete the mission, it is imperative that the aircraft be able to quickly reject disturbances such as wind gusts and return to its position within the Hover Station. To verify *Chezoía's* capability for this requirement, a case study was done for the aircraft in hover, suddenly hit by the maximum allowable wind gust allowed to maintain hover, 9.71 knots (5 m/s).

In this case, when struck by this gust from the side, the aircraft experiences a side force of about 18 lbs, derived from the aircaft's flat-plate area and the dynamic pressure associated with this wind speed. This force results in a sideways acceleration of 0.5805 ft/s^2 (0.177 m/s^2) which must be counteracted by a control maneuver. After detecting this disturbance, *Chezoía* begins a rolling maneuver, using 6% trim from its current control rotors. This begins a rolling angular acceleration of 4.5°/s^2 in order to begin to rotate the rotors' force vectors to combat the disturbance.

Integrating both the sideways accelerations from the wind and these lateral control forces results in intersection points when the aircraft will stop motion due to the wind and begin to return to its original position even assuming a one second controls delay to allow time for detection of the disturbance and execution of control maneuvers, this procedure shows that *Chezoía* will return to its original position within 14 seconds of being first hit by the gust and with a maximum displacement of only 2.05 feet (0.62 m). These control numbers were calculated using simple proportional control, not any advanced integral or derivative terms. The VECTOR’s advanced

PID control will be able to outperform these approximations due to these additional terms, as well as a faster response time to the initial disturbance.

This excellent control performance is possible with simple RPM control due to the multirotor design which reduces the size of each rotor. With significantly lower rotor inertia, the RPM control is capable of much faster response times than would be possible with fewer, larger rotors.

These calculations do not take into account rotor to rotor interference generated by sideways flight or the small rolling moment which would be created by the wind's side force. Both of these will slightly diminish the dynamic performance, however, this can be mitigated by the increased controllability resulting from canting the rotors inwards by 2°. This cant increases the aircrafts overall stability through force vectoring and only reduces the downward thrust of the rotors by 0.07%, an insignificant margin.

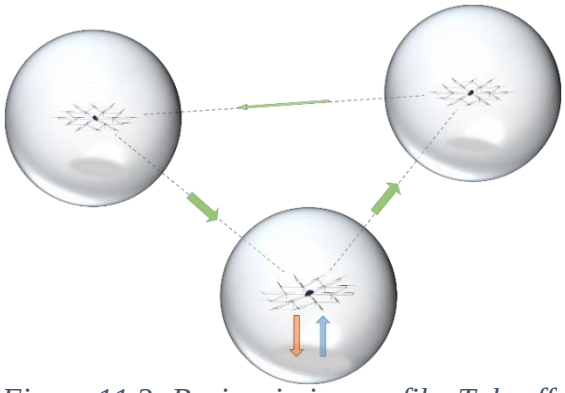

Figure 11.3: Basic mission profile. Takeoff (blue), cruise (green), HOGE (sphere), and landing (orange).

11.4 Mission Maneuvers

The main challenge presented by the RFP lies within the longevity of *Chezoía's* mission. However, maneuverability is still required in order to complete this mission. As can be seen in Figure 11.4, the mission has been divided into four basic essential maneuvering states, namely: (1) Takeoff, (2) Cruise, (3) Hover Outside of Ground Effect (HOGE), and (4) Landing.

11.4.1 Takeoff

Following remote startup, *Chezoía's* autopilot handles takeoff procedures to take the aircraft to an altitude of 150 feet (45 m). This maneuver will take about 30 seconds. During this time, the excess power required for climb reduces the available control trims to about half of the maximum trims that are allowable during other phases of the mission. This means that purely vertical ascent is not ideal in conditions with inconsistent or strong wind conditions. In these cases, the aircraft would instead take advantage of the benefits of inclined climb. In forward climb, the aircraft can ascend at the same rate, reaching cruising altitude within 30 seconds, while still maintaining the excess power available to execute maximum control maneuvers if necessary.

11.4.2 Cruise

Chezoía's cruise mechanics are similar to a simple quadcopter, due to the inspirations of its control scheme. In order to attain forward flight, the autopilot sets the desired attitude tilt the entire craft in the desired direction of flight, thus vectoring the thrust forces accordingly. During this forward flight, the maximum angle at which *Chezoía* can operate while maintaining altitude is 29°. This propels the aircraft laterally with an acceleration of 17.98 ft/s^2 (5.48 m/s^2). When in forward flight, the VECTOR responds to changes in rotor performance due to the advance ratio, and adjusts the control strategy accordingly, depending on the direction of each rotor and direction of flight.

Obstacle avoidance response: (1) avionics detect obstruction and relay to autopilot (2) Autopilot plots adjustment around obstruction and executes rolling maneuver (3) Aircraft returns to originally plotted flight path.

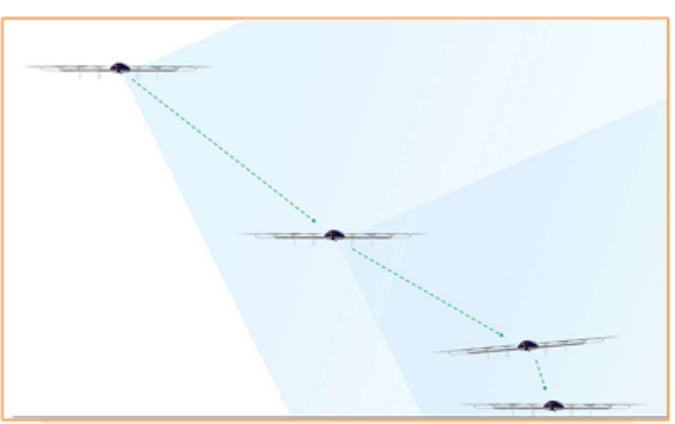

Decline landing procedure: blue shaded regions represent the vertical field of vision as the aircraft reaches the landing area, allowing for dynamic adjustment based on obstacles entering the area.

Chezoía's control scheme has been designed to take full advantage of the multirotor configuration for precision control, safety and mission assuredness through redundancy, as well as integrating a full obstacle avoidance suite for autonomous response to dynamic conditions.

Innovative quadcopter control sets offer:

- 3 fully redundant control systems
- Excellent controllability
- Minimal coupling between rotation controls

In addition, the 2° rotor cant further increases stability, with minimal losses for efficiency.

Through integration with *Chezoía's* sensor and avionics suite, all phases and maneuvers of the flight mission have full autonomous capability, allowing for a seamless endurance mission.

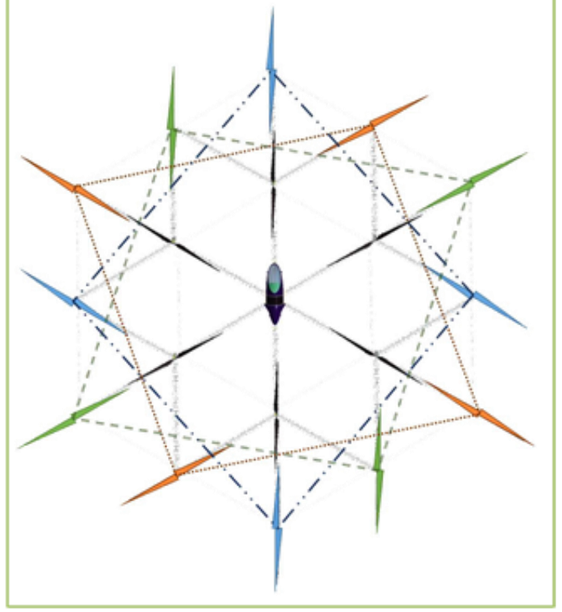

The quadcopter control sets allows three level redundancy throughout the craft's mission. The primary control set is in blue, while the secondary and tertiary sets (green and orange) can be switched to in the event that any primary control rotors are down for cooling or malfunction. Retains full control capabilities even with two or more rotors out. Each control set is designed to minimize coupling across roll, pitch, and yaw controls

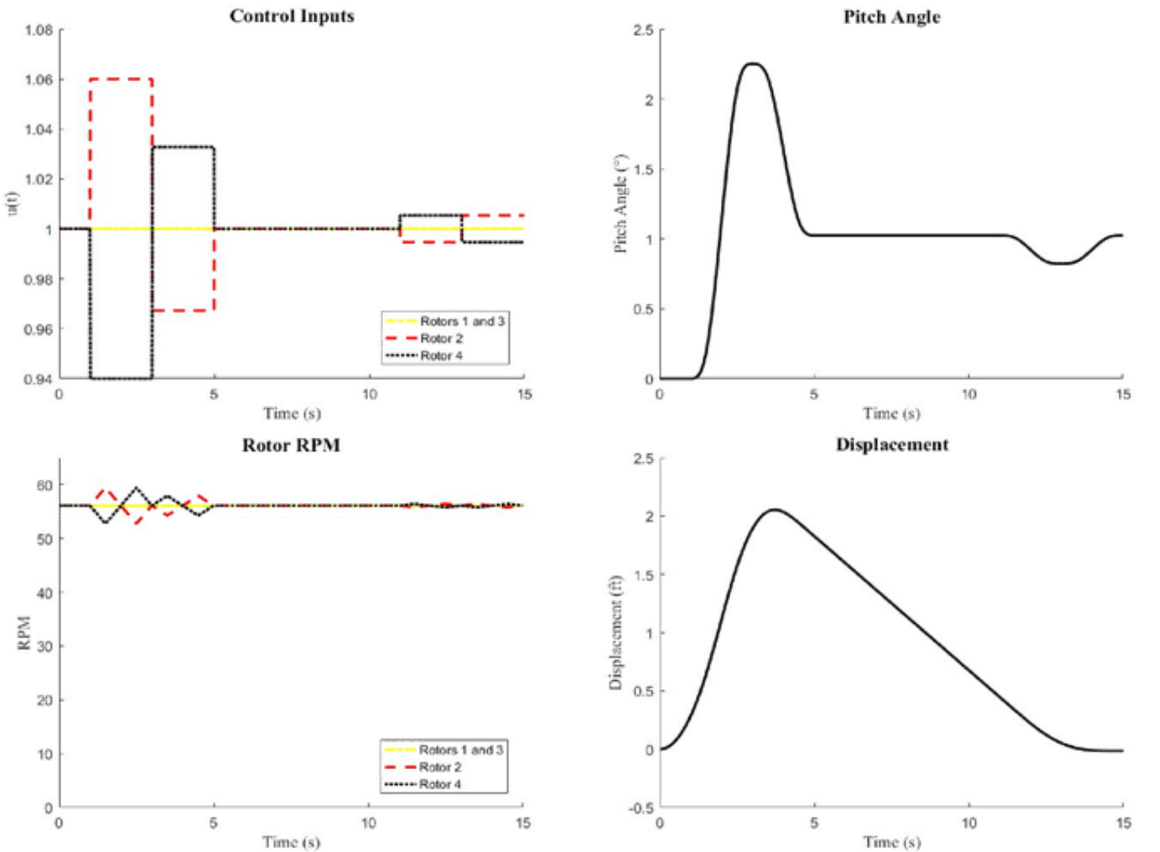

Basic control response to attenuate sudden constant wind of 9.71 knots. Craft returns to equilibrium at original position within 15 seconds with only 2 feet of maximum displacement

Periods of forward flight are determined prior to mission start, and a flight plan is preprogrammed into the VECTOR. With the advanced obstacle avoidance avionics, the vision processing CPU can detect obstacles on this path as they arise as described in Section 10.3.1, and transmit this data as no-fly zones to the VECTOR. Once the autopilot receives such an obstacle which is on its flight path, it will dynamically compute an avoidance maneuver to fly around the obstacle before returning to the originally planned flight path. This maneuver consists of either banking or pitching the aircraft to set a path either to the side or above the obstacle, depending on the dimensions of the no-fly zone and the aircraft's current altitude. Once this maneuver has been completed, the autopilot will return to the flight path that was originally specified and continue its mission.

As the aircraft approaches the next hover station, the autopilot monitors the aircraft's position relative to the prescribed hover station's position in order to slow to hover at the given location.

11.4.3 HOGE

During hover, it is essential that *Chezoía's* control scheme detects and responds effectively to disturbances such as wind. Since the time hovering must be spent with zero velocity relative to a fixed point on the ground, every second that the control scheme takes to return *Chezoía* to its original position and equilibrium adds to the total mission time. Efficiency is dependent on the aircraft's ability to maintain this equilibrium.

Chezoía's multirotor design facilitates this objective by increasing the responsiveness of RPM control. Due to the 18 rotors, each rotor is significantly smaller and therefore has much less inertia than the rotors necessary to complete the mission with other configurations. This lowered inertia allows the rotors to spin up or down according to control inputs significantly faster, increasing the effectiveness of the RPM control scheme. This response time was simulated as a conservative estimate in the calculations shown in the Dynamics and Controls foldout as taking a half second to adjust RPM by 6%.

Shown in the Dynamics and Controls foldout is an example response to attenuate a sudden change to the maximum hovering wind speed of 9.71 knots (5 m/s) as prescribed in the RFP. With this response, the control scheme brings the aircraft back to equilibrium in this wind speed within 14 seconds with a maximum displacement of only 2.05 ft (0.62 m). This conservative estimate is based on purely proportional control and allows for a one second delay after the wind starts before the autopilot responds. Both of these assumptions will be much improved by the VECTOR with its PID control and significantly faster response time. Using the same model with half the autopilot response time returns the craft to equilibrium in under 5.5 seconds with a maximum displacement under 1.2 feet (0.37 m). The VECTOR's derivative control term will outperform even this response time considerably, suggesting attenuation in under 5 seconds and less than 1 foot (0.3 m).

11.4.4 Landing

Upon completion of its hovering mission, the aircraft will begin the landing phase. During this maneuver, the craft will have travelled to the landing location in the original flight plan. On

approach to this location, the obstacle avoidance avionics will be able to identify any unplanned obstructions within the landing area and notify the autopilot to adjust as necessary.

There are two possible landing maneuvers. The first is a purely vertical landing which occurs once the aircraft hovers above the landing area. For this maneuver, the aircraft descends at a rate of 3 ft/s (0.91 m/s), keeping the rotors well out of the range of a vortex ring state. At this speed, the entire maneuver will take roughly one minute to complete. Using the lower extent of the obstacle avoidance viewing angles in conjunction with altitude information provided by the autopilot, the VECTOR will slow this descent further once the aircraft detects the ground within 10 feet (3.05 m), until it comes to a rest on the ground having completed the mission.

The second possible maneuver is the declined landing, which allows for better live identification of obstacles located at the landing area. The aircraft descends at an angle to maintain forward vision of the landing area throughout the landing process, allowing it to adjust if obstacles arise on the location. This maneuver is the preferred method of descent when vertical descent is not necessary due to surrounding conditions. Due to the redundancy built into the propulsion and controls systems with the multirotor design, either landing maneuver can be performed with up to 2 rotors out when at gross takeoff weight. By the end of the mission, having burned 220 lbs (100 kg) of fuel, landing maneuvers can still be completed with up to 5 rotors out.

12 Acoustics

12.1 Design for Low Noise

Chezoía's multirotor configuration does not require a tail rotor, so the majority of the vehicle's noise is produced by its many main rotors and diesel engine. The large number of rotors allows phasing of the rotors which will result in much less noise than a comparable single main rotor. The noise produced by the main rotors has four components: thickness noise, loading noise, High Speed Impulsive (HSI) noise and Blade Vortex Interaction (BVI) noise. HSI noise arises when the blade tips approach the speed of sound. HSI noise is not considered for this design because of the low tip speed of 0.42 Mach number at the tip. Blade vortex interaction (BVI) noise is the impulsive noise resulting from rapid pressure fluctuations as the blade passes near or through previously shed rotor vortices. BVI is insignificant for the majority of the mission because the vast majority is conducted in hover, so vortices will have minimal interaction with each other. In forward flight, however, BVI noise will be greatly increased because of the large number of rotors. Thickness noise arises because the finite thickness rotor blades displace fluid (air) as they rotate and translate through the medium. *Chezoía*'s blades are designed with a high degree of taper, so the thickness of the blade decreases rapidly across the span of the blade, so the thickness is very small towards the tip, reducing thickness noise. Loading noise is a function of thrust and *Chezoía*'s multirotor configuration reduces the thrust generated by each individual rotor, so the loading noise will be low. The noise produced by each rotor can be calculated using the Ffowcs-Williams and Hawking (FWH) equation, which only calculates thickness and loading noise, but is sufficient for *Chezoía*'s rotors. In hover, the noise signature is symmetric about the lateral plane, which is reflective of the arrangement of the rotors.

12.2 FAA Noise Requirements

Under the *Code of Federal Regulations, Title 14: Aeronautics and Space, Chapter I, Subchapter C, Part 36: Noise Standards: Aircraft Type and Airworthiness Certification,* helicopters are certified as Stage 1, Stage 2 and Stage 3. The Stage 3 helicopter noise standard was finalized in 2014 and applies to all new helicopter types certified after the implementation date of the rule. Under *Section J36.305 Noise Limits* [32], for vehicles under 7000 lb maximum takeoff weight (MTOW), the limit may be calculated by the equation:

$$L_{AE}(\text{limit}) = (82 + 3.0\,[\log_{10}(\text{MTOW}/1737)/\log_{10}(2)]\,)\ \text{dB}$$

For *Chezoía*'s MTOW of 1100 lb, the limit is ~80 dB across all stages of flight. This is lower than that which is required by Federal Aviation Administration rules

13 Failure Modes Analysis

Though *Chezoía* is unmanned, safety is still an important factor in design. Possible failure modes at each stage of operation were reviewed, and the cause, impact, and likelihood for each failure mode was identified and mitigated to ensure no excessive risks were taken in the design or operation of the aircraft.

13.1 Failure Modes, Effects, and Criticality Analysis

Failure Mode, Effects and Criticality Analysis (FMECA) was performed to identify the likelihood of a potential failure mode occurring and the impact of the failure on the system. Table 13.1 ranks the severity levels of a failure model from I-V, with I being catastrophic failure and V being an event of no concern. Probability of the occurrence of the failure modes are ranked form A-E, with A indicating very high probability (>75%) and E indication negligible probability (<10%). Therefore, a criticality level of I-A would necessitate immediate attention and resolution of the problem while V-E would be low on a priority list. Descriptions of these probability levels can be found below in Table 13.2.

Table 13.1: Severity levels of a potential failure mode.

Severity Level Description	
I	Catastrophic - Injury or loss of life possible
II	Major Concern - Vehicle not recoverable/repairable
III	Moderate Concern - Mission failure
IV	Low Concern - Mission effectiveness reduced
V	No concern

Table 13.2: Probability of occurrence of any particular failure mode.

Probability Level	
A	Very High Probability (>75%)
B	High Probability (50-75%)
C	Moderate Probability (25-50%)
D	Low Probability (5-25%)
E	Negligible Probability (<5%)

Table 13.3: Identified failure modes and mitigation strategies

RISK	SEVERITY	LIKELIHOOD	CONSEQUENCES	MITIGATION
One engine out	II	D	Crash landing of vehicle	Emergency battery
Total power loss	I	E	Crash landing of vehicle	Emergency battery
Unexpected weather/wind	IV	B	Decreased control, rotor stall	Adjust other rotors to compensate lift and control
Vector failure	II	E	Loss of navigation and control	Internal redundancies, and emergency battery
Telem05 failure	IV	D	Loss of communication with ground station	Either continue with autonomous mission, or begin landing procedure
Temperature sensor failure	IV	E	Overheating of rotors, loss of motors	Adjust other rotors to compensate lift and control
Current sensor failure	IV	E	Loss of ability to adjust for rotor failure	Adjust other rotors to compensate lift and control
LED failure	V	D	Loss of visual detection by other aircraft	Multiple LEDs installed
Monocular camera failure	III	D	Reduced or loss of vision	Multiple visual cameras installed
Processor failure	III	D	Loss of object sensing	Begin landing procedure, or continue with preprogrammed flight plan
Thermal camera failure	IV	D	Loss of low-light visibility, collision with transient object	Multiple thermal cameras installed. LiDAR system installed
LiDAR failure	V	D	Loss of redundant system	Use thermal cameras, if both systems down, automatic landing of vehicle
ADS-B failure	IV	D	Collision with other aircraft	Automatic return to base
Airframe structural failure	II	D	Loss of rotor, vehicle imbalance, crash landing of vehicle	Structure sized to withstand 1.5 expected loads
One blade failure	III	D	Loss of lift	Adjust other rotors to compensate lift and control
One gearbox failure	III	C	Loss of lift	Adjust other rotors to compensate lift and control
Control algorithm failure	I	E	Flight instability, crash landing of vehicle	Emergency battery

Table 13.3 shows a list of potential failure models identified and analyzed for *Chezoía*. This list contains primarily the vehicle level failure modes, such as one engine out, failure of delivery mechanism, faulty communication system, etc. The failure modes were identified based on severity and likelihood. Potential consequences and the effects on mission performance were analyzed. Finally, a mitigation strategy, i.e., system or component solutions developed, were implemented as part of the *Chezoía* system to reduce the criticality levels and promote safety.

There are no A-I events, and the level-I events have a low likelihood of occurring. Therefore, the system has adequate safety.

13.2 Downwash and Disk Loading

High rotor downwash can generate high speed debris when near unprepared surfaces. This debris can cause harm to the vehicle and any surrounding personnel, and therefore, should be avoided. *Chezoía*'s downwash velocity is low enough to be safe to operate near people. The kinetic energy of each blade is also low enough so that a blade striking a person is not lethal, making it safe in crowded environments; however, precautions will be taken to ensure no persons are in the vincinity of *Chezoía* during normal operations.

14 Cost Breakdown

The total cost of *Chezoía* includes the development cost, production cost, operational cost, and end of life cost. Considered below are the development and production costs associated with manufacturing one aircraft. Additional considerations should be made for the cost of component testing, operational costs such as inspections and crew, and end of life costs for non-recyclable components.

The cost of *Chezoía's* components can be seen in Table 14.1. Within this cost consideration is included the initial purchase price of each component and the cost of fabrication and labor (priced at $90 per manhour). These calculations were done using The Official Helicopter Blue Book. These considerations bring the production cost of *Chezoía* to just under half a million dollars at $482,260. Major contributions to this figure are made from the labor cost for the microtruss structure and fuselage, as well as the manufacturing of blades.

Table 14.1: Chezoía Production Cost.

Component	Cost
Blades and Hubs	$118,800
Microtruss Structure	$135,245
Center Section	$100,000
Landing Gear	$20,160
Engine	$30,000
Generator	$6,800
Radiator	$500
Motors	$21,800
Gearboxes	$26,840
ESCs	$1,854
Avionics	$20,075
Fuel	$186
Total	**$482,260**

15 Weight Analysis

Chezoía was designed as a lightweight vehicle to reduce the fuel and resulting mission costs. As a result, the payload and fuel make up a moderate fraction of the vehicle weight. The resulting empty weight fraction of the vehicle is 0.604. A breakdown of the weights of different components and their weights can be seen in Table 15.1.

Table 15.1: Component weight breakdown.

COMPONENT		WEIGHT (LBS)	WEIGHT (KG)	% EMPTY WEIGHT	X_{CG} (IN)	X_{CG} (M)
1 ROTORS		**140**	**63.636**	**23.61**		
2 STRUCTURE		**281**	**127.73**	**47.39**		
	Trusses	176	80	29.68	0	0
	Center Section	105	47.73	17.71	3.5	0.089
3 LANDING GEAR		**7**	**3.18**	**1.18**		
4 PROPULSION		**179.14**	**81.43**	**29.18**		
	Engine	70	31.75	12.14	-17.5	-0.444
	Generator and Controller	30.38	13.81	5.12	-26	-0.660
	Radiator/Fan	5	2.27	0.84	-28	-0.711
	Cooling Tower	10	4.54	1.69	-30	-0.762
	Motors	11.64	5.292	1.96	0	0
	Gearboxes	24.8	11.28	4.18	0	0
	ESCs	4.32	1.962	0.73	0	0
	Emergency Battery	21	11.2788	3.42	-30	-0.762
5 AVIONICS		**6.842**	**3.110**	**1.15**		
	Autopilot	0.397	0.18	0.07	0	0
	CPU	3.439	1.56	0.58	11	0.279
	Communications	0.617	0.28	0.10	0	0
	Cameras Fore	0.158	0.072	0.03	49.5	1.257
	Cameras Mid/Lidar	0.340	0.154	0.06	11	0.279
	Cameras Aft	0.037	0.017	0.01	-37.5	-0.952
	Monitoring	0.794	0.36	0.13	0	0
	Auxiliary Battery	1.060	0.482	0.18	0	0
6 PAYLOAD		**176.4**	**80.18**	**-**	**15.5**	**0.394**
7 FUEL		**220**	**100**	**-**	**0**	**0**
	Total	**1003.38**		**100.00**		

The weight distribution of all the components was designed to ensure that the center of gravity remains as close as possible to the geometric center of the vehicle. Since *Chezoía*'s unique configuration allows for large stabilizing moment arms provided by the external rotors, the center of gravity envelope for the vehicle is relatively large and can be seen in Figure 15.1. The center of gravity for the 24-hour hover mission begins at 0.65 inches (16.51 mm) forward of the geometric center, and remains unchanged as the vehicle burns fuel.

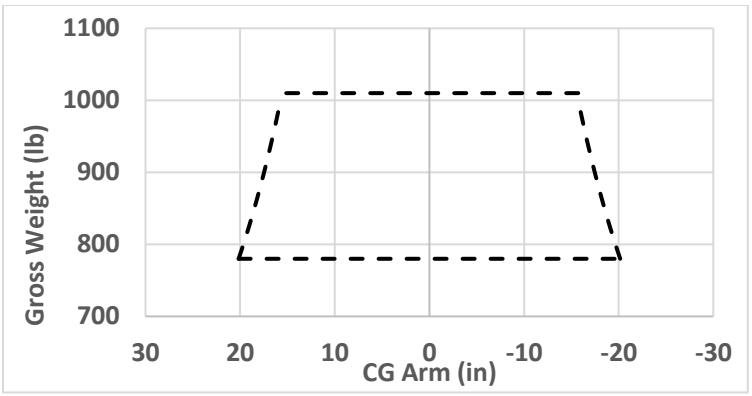

Figure 15.1: Longitudinal center of gravity envelope for Chezoía.

16 Summary

Through careful calculations and considerations, as well as leveraging available technologies to develop its innovative configuration, *Chezoía* offers an efficient, safe, and effective solution to a wide variety of possible missions. As a highly deployable and versatile aircraft, the proposed design features:

Capability for 25 hours of hover: Designed for efficiency in hover, *Chezoía* has been optimized specifically for this mission at every stage, from configuration to rotor design. The 18 rotor design allows for a disk loading of 0.61 lb/ft^2, while the structural weight is kept low by the microtruss system. At the same time, the blades were designed to an excellent figure of merit of 0.803. Together, these parameters allow for a craft which exceeds expectations with 25 hours of hover.

Precision control: Throughout the course of its fully autonomous mission, *Chezoía* maintains precise control and excellent disturbance response in both hover and forward flight. These allow for less time to be spent correcting position, and more time spent toward the completion of its mission. The proven quad-rotor control scheme, along with advanced vision and obstacle avoidance techniques, maximize the efficiency of time during the course of flight.

Safety and assuredness through redundancy: *Chezoía* ensures the success and safety of its mission with the careful design of its most important systems. The rotor system's motors and gearboxes have been sized with redundancy of a minimum of two rotors at gross take-off weight, while the innovative quadcopter control sets allow for the same level of redundancy while maintaining full control capabilities. Through redundancies, *Chezoía* is able to continue and complete missions after failures that would ground or incapacitate other aircraft.

Highly modular design: The modularity of *Chezoía's* design allows for excellent deployability through the transportability of its full assembly kit. In addition, it further allows for ease of maintenance and rapid replacement of parts. Maintenance is further simplified through the system of diagnostic information streamed from the avionics suite to the central fuselage. All of this contributes to the overall ease of use for the vehicle.

Readiness: The systems and technologies explored within *Chezoía's* design have been based on conservative studies with currently available hardware, software, and algorithms. Due to these considerations, the necessary components are readily available to facilitate *Chezoía's* immediate success, allowing for accelerated usage timelines and developmental cost savings.

Versatility and adaptability to new missions: The aircraft has been designed with a variety of applications and uses throughout the process, ranging from an autonomous testing platform, to a central drone mothership, as well as commercial or paramilitary applications as well. With these considerations, as well as the ease of transitioning to a piloted flight, *Chezoía* is ready for whatever missions may be necessary.

17 References

[1] T. Saaty, "Decision Making With the Analytic Hierarchy Process," *International Journal of Services Sciences,* vol. 1, no. 1, pp. 83-98, 2008.

[2] M. Benedict, "Development of 200 gram twin-rotor micro cyclocopter capable of autonomous hover," in *American Helicopter Society Future Vertical Lift Aircraft Design Conference*, San Francisco, CA, 2012.

[3] M. Tishchenko, V. T. N. "ENAE634 Helicopter Design Lecture Notes," University of Maryland, College Park, 2008.

[4] W. Johnson, "NDARC — NASA Design and Analysis of Rotorcraft," NASA Aeromechanics Branch, Moffett Field, 2010.

[5] C. A. Snyder, "Exploring propulsion system requirements for more and all-electric helicopters," in *International Symposium on Air Breathing Engines*, Phoenix, AZ, 2015.

[6] "R22 Introduction and Specifications," Robinson, [Online]. Available: https://robinsonheli.com/r22-specifications/. [Accessed 19 May 2017].

[7] J. Schmaus, "Design and Development of Gamera: A Human Powered Helicopter from the University of Maryland," American Helicopter Society International, Inc., 2012.

[8] M. Drela, " XFOIL: An Analysis and Design System for Low Reynolds Number Airfoils.," in *Low Reynolds Number Aerodynamics. Lecture Notes in Engineeringg, vol 54*, Springer, Berlin, Heidelberg, 1989.

[9] S. A. Corporation, "Airfoil for a helicopter rotor blade". Patent US 7854593 B2, 21 December 2010.

[10] M. S. Selig, "Low Reynolds Number Airfoil Design," von Karman Institute for Fluid Dynamics, Sint-Genesius-Rode, 2003.

[11] W. Johnson, Rotorcraft Aeromechanics, New York: Cambridge University Press, 2013.

[12] W. Staruk, "Design and Fabrication of Ultra-Lightweight Composite Structures for the

Gamera Human-Powered Helicopter," American Helicopter Society International, Inc., 2012.

[13] B. Riley, "Anthropomorphic Reference Data," Formula SAE, 2015.

[14] S. F. Hoerner, Fluid Dynamic Drag, Bakersfield, CA, 1965.

[15] D. Stock and R. Bauder, "The New Audi 5-Cylinder Turbo Diesel Engine: The First Passenger Car Diesel Engine with Second Generation Direct Injection," SAE, 1990.

[16] Turnigy, "Hobby King," [Online]. [Accessed May 2017].

[17] SUNON, "How to Select the Right Fan or Blower," [Online]. Available: http://www.sunon.com/uFiles/file/03_products/07-Technology/004.pdf. [Accessed May 2017].

[18] J. Madej and B. Bedkowski, "Air Flow Analysis for Electrical Motor's Cooling System with Autodesk Simulation CFD 2013 Program," *Acta Mechanica et Automatica,* vol. 7, no. 2, pp. 89-92, 2013.

[19] UAV Navigation, "VECTOR," [Online]. Available: http://www.uavnavigation.com/products/autopilots/vector. [Accessed May 2017].

[20] UAV Navigation, "TELEM05," [Online]. Available: http://www.uavnavigation.com/support/kb/peripherals/datalinks/datalink-900-mhz/telem05.

[21] TE Connectivity, "DDEController," October 2015. [Online]. Available: http://www.te.com/commerce/DocumentDelivery/DDEController [Accessed May 2017].

[22] Eaton, "DC Current Sensor," [Online]. Available: http://www.eaton.com/Eaton/ProductsServices/Electrical/ProductsandServices [Accessed May 2017].

[23] Federal Aviation Administration, *Federal Aviation Regulations §23.1389,* Washington DC.

[24] D. Caruso J. E., "Large-Scale Direct SLAM for Omnidirectional Cameras," 2015.

[25] Matrix Vision, "USB 2.0 camera - mvBlueFOX," 2017. [Online]. Available: https://www.matrix-vision.com/USB2.0-industrial-camera-mvbluefox.html. [Accessed May 2017].

[26] J. Engel S. J. C. D., "Semi-Dense Visual Odometry for a Monocular Camera".

[27] Sparton, "LPC-480G4 – Powerful Mini PC with Multi Gigabit LAN," 2017. [Online]. Available:

https://www.spartonre.com/littlepcs/high-performance-mini-pcs/ [Accessed May 2017].

[28] FLIR, "Quark 2 Uncooled Cores," 2017. [Online]. Available:

http://www.flir.com/cores/display/?id=51266. [Accessed May 2017].

[29] Scanse, "Sweep V1 360° Laser Scanner," 2017. [Online]. Available: http://www.robotshop.com/media/files/pdf2/user_s_manual_sweep_v0.91.pdf. [Accessed May 2017].

[30] Federal Aviation Administration, *Automatic Dependent Surveillance--Broadcast (ADS-B)*

Out Performance Requirements To Support Air Traffic Control (ATC) Service §91.225,

Washington DC, 2010.

[31] S. C. Engel, "LSD-SLAM: Large-Scale," 2014.

[32] Federal Aviation Administration, " Title 14: Aeronautics and Space," [Online].

Available: https://www.ecfr.gov/. [Accessed 5 May 2017].

[33] Emrax, "EMRAX 208 User's Manual," 2017. [Online]. Available: http://emrax.com/wp-content/uploads/2017/01/emrax_208_technical_data_4.5.pdf.

[34] P. Giguere and M. S. Selig, "New Airfoils for Small Horizontal Axis Wind Turbines," *Journal of Solar Energy Engineering,* vol. 120, pp. 108-114, 1998.

[35] AHS International, “24 Hour Hovering Machine Conceptual Design – Request for Proposals”